Ushijima T, Sasako M. (2004). *Cancer Cell* **5**: 121–125.
Visse R, Nagase H. (2003). *Circ Res* **92**: 827–839.
Yamashita K, Azumano I, Mai M, Okada Y. (1998). *Int J Cancer* **79**: 187–194.
Yasui W, Oue N, Ito R, Kuraoka K, Nakayama H. (2004). *Cancer Sci* **95**: 385–392.
Yasui W, Yokozaki H, Fujimoto J, Naka K, Kuniyasu H, Tahara E. (2000). *J Gastroenterol* **35**: 111–115.
Zhang X, Huang Q, Yang Z, Li Y, Li CY. (2004). *Cancer Res* **64**: 2474–2481.
Zucker S, Hymowitz M, Conner C, Zarrabi HM, Hurewitz AN, Matrisian L *et al*. (1999). *Ann N Y Acad Sci* **878**: 212–227.

Supplementary Information accompanies the paper on the Oncogene website (http://www.nature.com/onc)

Journal of Pathology
J Pathol 2006; **208**: 633–642
Published online 24 January 2006 in Wiley InterScience (www.interscience.wiley.com). **DOI:** 10.1002/path.1922

Original Paper

Down-regulation of the claudin-18 gene, identified through serial analysis of gene expression data analysis, in gastric cancer with an intestinal phenotype

Y Sanada,[1,2] N Oue,[1] Y Mitani,[1] K Yoshida,[2] H Nakayama[1] and W Yasui[1]*
[1]*Department of Molecular Pathology, Hiroshima University Graduate School of Biomedical Sciences, Hiroshima, 734-8551, Japan*
[2]*Department of Surgical Oncology, Research Institute for Radiation Biology and Medicine, Hiroshima University, Hiroshima, 734-8551, Japan*

*Correspondence to:
W Yasui, Department of Molecular Pathology, Hiroshima University Graduate School of Biomedical Sciences, 1-2-3 Kasumi, Minami-ku, Hiroshima, 734-8551, Japan.
E-mail: wyasui@hiroshima-u.ac.jp

Received: 9 September 2005
Revised: 15 October 2005
Accepted: 1 November 2005

Abstract

Gastric cancer (GC) is one of the most common malignancies worldwide. Genes whose expression is down-regulated in GC may be tumour suppressor genes. In the present study, genes with decreased expression in GC were screened for by serial analysis of gene expression (SAGE) data analysis and reverse transcription (RT)-polymerase chain reaction (PCR), and *CLDN18* (encoding claudin-18) was identified. Quantitative RT-PCR revealed that expression of *CLDN18* was down-regulated in 13 (56.5%) of 23 GCs. Immunostaining showed that normal gastric mucosa and Paneth cells of the duodenum expressed claudin-18 on cell membranes. Expression of claudin-18 was reduced in several intestinal metaplasias of the stomach. Of 20 samples of gastric adenoma, 18 (90.0%) showed decreased claudin-18 expression. Down-regulation of claudin-18 was observed in 84 of 146 GCs (57.5%) and correlated with poor survival in 65 advanced GCs ($p = 0.0346$). In addition, expression of the gastric and intestinal phenotypes of GC was examined by immunostaining for MUC5AC, MUC6, MUC2, and CD10. Of 38 GCs showing only the intestinal phenotype, down-regulation of claudin-18 was observed in 28 (73.7%), whereas in the remaining 108 GC cases, down-regulation of claudin-18 was observed in 56 (51.9%) ($p = 0.0224$). These results indicate that claudin-18 is a good marker of poor survival in GC. Down-regulation of claudin-18 may be involved in GCs with an intestinal phenotype, and may be an early event in gastric carcinogenesis.

Copyright © 2006 Pathological Society of Great Britain and Ireland. Published by John Wiley & Sons, Ltd.

Keywords: claudin-18; gastric cancer; phenotype expression; serial analysis of gene expression; SAGE

Introduction

Cancer develops as a result of multiple genetic and epigenetic alterations [1,2]. Better knowledge of the changes in gene expression that occur during gastric carcinogenesis may lead to improvements in diagnosis, treatment, and prevention. We previously performed serial analysis of gene expression (SAGE) on four primary gastric cancer (GC) samples (Gene Expression Omnibus accession number GSE 545; SAGE Hiroshima gastric cancer tissue) and identified several genes and tags that are potentially involved in invasion, metastasis, and carcinogenesis [3]. In the present study, to identify genes with down-regulation of expression in GC, we screened GC SAGE libraries and identified several candidate genes. Among them, *CLDN18*, which encodes claudin-18, was found by quantitative reverse transcription (RT)-polymerase chain reaction (PCR) to be frequently down-regulated in GC. However, little is known about *CLDN18* and cancer.

The claudin protein family comprises 24 members, and all claudins are 20–27 kD proteins with four transmembrane domains [4]. Members of the claudin family are involved in various biophysiological processes, such as regulation of paracellular permeability and conductance. Several reports have suggested an association between claudin and cancer [5]. *CLDN18* was first identified as a downstream target gene of the T/EBP/NKX2.1 homeodomain transcription factor [6]. *CLDN18* has been reported to have two variants in mice: variant 1 (*CLDN18a1*) is expressed in the lung, whereas variant 2 (*CLDN18a2*) is expressed in the stomach.

The present study represents the first detailed analysis of *CLDN18* expression in human cancer. To clarify the pattern of expression and localization of claudin-18 in GC, we performed immunohistochemical analysis of surgically resected GC samples. In addition, because we observed frequent down-regulation of claudin-18 in intestinal metaplasia of the stomach, we investigated the association between claudin-18

Copyright © 2006 Pathological Society of Great Britain and Ireland. Published by John Wiley & Sons, Ltd.

expression and expression of the gastric or intestinal phenotype of GC.

Materials and methods

GC cell lines

Eight cell lines derived from human GC were used. The TMK-1 cell line was established in our laboratory from a poorly differentiated adenocarcinoma [7]. Five GC cell lines of the MKN series (MKN-1, adenosquamous cell carcinoma; MKN-7; MKN-28; MKN-74, well-differentiated adenocarcinoma; and MKN-45, poorly differentiated adenocarcinoma) were kindly provided by Dr Toshimitsu Suzuki. KATO-III and HSC-39 cell lines, which were established from signet ring cell carcinomas, were kindly provided by Dr Morimasa Sekiguchi and Dr Kazuyoshi Yanagihara, respectively [8]. All cell lines were maintained in RPMI 1640 (Nissui Pharmaceutical Co, Ltd, Tokyo, Japan) containing 10% fetal bovine serum (BioWhittaker, Walkersville, MD, USA) in a humidified atmosphere of 5% CO_2 and 95% air at 37 °C.

Tissue samples

For quantitative RT-PCR, 23 GC tissue cases were used. The samples were obtained at the time of surgery at Hiroshima University Hospital or an affiliated hospital. We confirmed microscopically that the tumour specimens consisted mainly (>80%) of carcinoma tissue. Samples were frozen immediately in liquid nitrogen and stored at −80 °C until use. Non-neoplastic samples of heart, lung, stomach, small intestine, colon, liver, pancreas, kidney, bone marrow, peripheral leukocytes, spleen, skeletal muscle, brain, and spinal cord were purchased directly from Clontech (Palo Alto, CA, USA).

For immunohistochemical analysis, we used archival formalin-fixed, paraffin-embedded tissues from 146 patients who had undergone surgical excision for GC. The 146 GC cases were histologically classified as well or poorly differentiated. Tumour staging was carried out according to the TNM staging system [9]. Because written informed consent was not obtained, identifying information for all samples was removed before analysis for strict privacy protection; this procedure was in accordance with the Ethical Guidelines for Human Genome/Gene Research enacted by the Japanese Government.

Screening of SAGE libraries for genes with expression down-regulated in GC

To identify genes with decreased expression in GC, we used two GC SAGE libraries (W226T, GSM8867; W246T, GSM8505) made by us [3] and one normal stomach SAGE library (stomach, GSM784) [10] available from the SAGEmap online database (http://www.ncbi.nlm.nih.gov/SAGE/) [11]. We compared tags from each GC SAGE library with those of the normal stomach SAGE library and selected tags that were down-regulated in the GC SAGE libraries. To exclude tags generated by sequencing errors, we selected only tags that occurred at least twice in the normal stomach SAGE library. In addition, we selected genes that had not been investigated previously (Table 1).

Conventional and quantitative RT-PCR analyses

Total RNA was extracted with an RNeasy Mini Kit (Qiagen, Valencia, CA, USA) and 1 μg of total RNA was converted to cDNA with a First Strand cDNA Synthesis Kit (Amersham Biosciences, Piscataway, NJ, USA). The amplification products were then separated by 1% agarose gel electrophoresis, stained with ethidium bromide, and visualized under UV light. *ACTB*-specific PCR products served as internal controls. The primer sequences for variant-specific expression of *CLDN18* and annealing temperatures are listed in Table 2. Other primer sequences and additional PCR conditions are available upon request.

Quantitation of *CLDN18* mRNA levels in human tissue samples was performed with real-time fluorescence detection as described previously [12]. Sequences of primers and annealing temperatures are described in Table 2. PCR was performed with an SYBR Green PCR Core Reagents Kit (Applied Biosystems, Foster City, CA, USA). Real-time detection of the emission intensity of SYBR Green bound to double-stranded DNA was carried out with an ABI PRISM 7700 Sequence Detection System (Applied Biosystems) as described previously [13]. *ACTB*-specific PCR products were amplified from the same RNA samples and served as internal controls. We calculated the ratio of *CLDN18* mRNA levels between GC tissue (T) and corresponding non-neoplastic mucosa (N). T/N ratios of less than 0.5 were considered to indicate down-regulation.

Subcloning and sequencing

PCR products were purified and cloned into the pCR2.1 vector (Invitrogen, Carlsbad, CA, USA). Plasmid DNA was extracted from individual clones by alkaline lysis plasmid mini-preparation. The inserted PCR fragments obtained from each sample were sequenced with M13 reverse and M13 forward primers with the PRISM AmpliTaq DNA Polymerase FS Ready Reaction Dye Terminator Sequencing Kit (Applied Biosystems). Reamplified DNA fragments were purified with Centri-sep Columns (Applied Biosystems) and sequenced with an ABI PRISM 310 Genetic Analyzer (Applied Biosystems).

Antibodies

Anti-claudin-18 antibody (C-term) was purchased from Invitrogen. We used four antibodies for analysis

Table 1. List of genes and tags with reduced expression in GC

Tag sequence	Tags per million: Normal stomach (25 302*)	Tags per million: GC W226T (43 908*)	Tags per million: GC W246T (32 174*)	Symbol	Description
TCCCCTACAT	553† (14)‡	0 (0)	62 (2)	*ADAMTS16*	A disintegrin-like and metalloproteinase (reprolysin type) with thrombospondin type 1 motif, 16
TATTTCACTT	395 (10)	22 (1)	0 (0)	*KNSL8*	Kinesin-like 8
AAACCCCGTC	316 (8)	45 (2)	0 (0)	*KIAA0682*	KIAA0682 gene product
GTGGTACAGG	276 (7)	0 (0)	62 (2)	*KIFC3*	Kinesin family member C3
CTCATTCAGC	276 (7)	45 (2)	0 (0)	*SMT3H2*	SMT3 suppressor of mif two 3 homologue 2 (yeast)
CCCCTCCCTC	237 (6)	22 (1)	0 (0)	*API5*	Apoptosis inhibitor 5
GGGAGCCCCT	197 (5)	45 (2)	0 (0)	*ARRB2*	Arrestin, beta 2
GATTCCTTTG	197 (5)	0 (0)	0 (0)	*CHES1*	Checkpoint suppressor 1
GTTACAAGCC	197 (5)	22 (1)	0 (0)	*CLDN18*	Claudin 18
CTGATTTATT	197 (5)	0 (0)	62 (2)	*COPG*	Coatomer protein complex, subunit gamma
GCTAAACAGG	197 (5)	0 (0)	0 (0)	*EIF3S10*	Eukaryotic translation initiation factor 3, subunit 10 theta, 150/170 kD
GACATCGAGG	197 (5)	0 (0)	0 (0)	*KIF4A*	Kinesin family member 4A
CCCATAGTCC	197 (5)	0 (0)	0 (0)	*RAB4B*	RAB4B, member RAS oncogene family
AACCCGGAAG	158 (4)	22 (1)	31 (1)	*BTN3A2*	Butyrophilin, subfamily 3, member A2
AACCCGGAAG	158 (4)	22 (1)	31 (1)	*FLJ31819*	Hypothetical protein FLJ31819
AAGCCCAGGC	158 (4)	45 (2)	62 (2)	*MR-1*	Myofibrillogenesis regulator 1
AAGATACTGA	118 (3)	0 (0)	0 (0)	*SLC30A9*	Solute carrier family 30 (zinc transporter), member 9
AAGATACTGA	118 (3)	0 (0)	0 (0)	*COPB*	Coatomer protein complex, subunit beta
AACCACCACG	79 (2)	0 (0)	0 (0)	*C7*	Complement component 7
AAAACTTCTC	79 (2)	0 (0)	0 (0)	*FLJ10849*	Hypothetical protein FLJ10849
AAAACTTCTC	79 (2)	0 (0)	0 (0)	*MOB4A*	Mob4A protein
AAACTGTTCA	79 (2)	0 (0)	31 (1)	*KIAA0256*	KIAA0256 gene product
AAGACTGAAG	79 (2)	0 (0)	31 (1)	*PDCD8*	Programmed cell death 8 (apoptosis-inducing factor)
AAGACTGAAG	79 (2)	0 (0)	31 (1)	*RDH14*	Retinol dehydrogenase 14 (all-*trans* and 9-*cis*)
AAATATGAAG	79 (2)	0 (0)	0 (0)	*SEC22L1*	SEC22 vesicle trafficking protein-like 1 (*S. cerevisiae*)

* Total number of tags.
† The absolute tag counts are normalized to 1 000 000 total tags per sample.
‡ Numbers in parentheses indicate the absolute tag counts.

Table 2. Primer sequences for conventional and quantitative RT-PCR

Primer sequence	Annealing temperature (°C)	Size (bp)
First screening primers for *CLDN18*		
F: 5′-GTGGAGCACCCAGGACCTGTA-3′	55	500
R: 5′-AGGCGATGCACATCATCACAC-3′		
CLDN18 variant 1-specific primers		
F: 5′-CAGGATCATGTCCACCACCACA-3′	60	818
R: 5′-GCCCGTGCTGAGAGGTCTTAGA-3′		
CLDN18 variant 2-specific primers		
F: 5′-CGCTGTCCACTTGTCGTGTG-3′	66	880
R: 5′-TGAGCTCTCCGGGAGTTTCTTC-3′		
ACTB for conventional RT-PCR		
F: 5′-CTGTCTGGCGGCACCACCAT-3′	55	254
R: 5′-GCAACTAAGTCATAGTCCGC-3′		
CLDN18 for quantitative RT-PCR		
F: 5′-GATCGTAGGCATCGTCCTGG-3′	60	65
R: 5′-GGATGCATTTCAGGGCAAAG-3′		
ACTB for quantitative RT-PCR		
F: 5′-TCACCGAGCGCGGCT-3′	60	60
R: 5′-TAATGTCACGCACGATTTCCC-3′		

of the GC phenotypes: anti-MUC5AC (Novocastra, Newcastle, UK) as a marker of gastric foveolar epithelial cells, anti-MUC6 (Novocastra) as a marker of pyloric gland cells, anti-MUC2 (Novocastra) as a marker of goblet cells in the small intestine and colorectum, and anti-CD10 (Novocastra) as a marker of microvilli of absorptive cells in the small intestine and colorectum.

Western blot analysis

For western blot analysis, cells were lysed as described previously [14]. The lysates (40 μg) were solubilized in Laemmli sample buffer by boiling and then subjected to 12% SDS-polyacrylamide gel electrophoresis followed by electrotransfer onto a nitrocellulose filter. Peroxidase-conjugated anti-rabbit IgG was used in the secondary reaction. Immune complexes were visualized with an ECL Western Blot Detection System (Amersham Biosciences).

Immunohistochemistry

A Dako LSAB Kit (Dako, Carpinteria, CA, USA) was used for immunohistochemical analysis. In brief, sections were pretreated by microwave treatment in citrate buffer for 15 min to retrieve antigenicity. After peroxidase activity was blocked with 3% H_2O_2–methanol for 10 min, sections were incubated with normal goat serum (Dako) for 20 min to block non-specific antibody binding sites. Sections were incubated with the following primary antibodies: anti-claudin-18 (diluted 1 : 100), anti-MUC5AC (1 : 100), anti-MUC6 (1 : 100), anti-MUC2 (1 : 100), and anti-CD10 (1 : 100). Sections were incubated with primary antibody for 1 h at 25 °C, followed by incubations with biotinylated anti-rabbit/mouse IgG and peroxidase-labelled streptavidin for 10 min each. Staining was completed with a 10-min incubation with the substrate–chromogen solution. The sections were counterstained with 0.1% haematoxylin.

Claudin-18 staining was classified according to the percentage of stained cancer cells. Expression was considered to be 'down-regulation' if less than 50% (0–10%, 0; 10–50%, 1+) of cancer cells were stained. When at least 50% (50–80%, 2+; more than 80%, 3+) of cancer cells were stained, the immunostaining was considered 'not down-regulated'.

Phenotypic analysis of GC

GC cases were classified into four phenotypes: gastric (G) type, intestinal (I) type, gastric and intestinal mixed (GI) type, and unclassified (N) type. The criteria [15] for classification of G type and I type were as follows. GCs in which more than 10% of the cells displayed the gastric or intestinal epithelial cell phenotype were classified as G-type or I-type cancers, respectively. Those sections that showed both gastric and intestinal phenotypes were classified as GI type, and those that lacked both the gastric and the intestinal phenotypes were classified as N type.

Statistical methods

Correlations between clinicopathological parameters and claudin-18 expression were analysed by Fisher's exact test. Kaplan–Meier survival curves were constructed for claudin-18-positive and claudin-18-negative patients. Survival rates were compared between claudin-18-positive and claudin-18-negative groups. The differences in survival curves between groups were tested for statistical significance by the log-rank test [16]. p values of less than 0.05 were considered statistically significant.

Results

Identification of down-regulated genes in GC through analysis of SAGE data

To identify genes with decreased expression in GC, we screened SAGE libraries. We compared tags from two GC SAGE libraries with those of a normal stomach SAGE library and selected tags that were down-regulated in the GC SAGE libraries. To exclude tags generated by sequencing errors, we selected only tags that occurred at least twice in the normal stomach SAGE library. Down-regulated genes in the GC libraries included *ADAMTS16*, *KNSL8*, and *KIFC3*. We then investigated the expression of the candidate down-regulated genes listed in Table 1 by conventional RT-PCR analysis in eight GC cell lines (representative results are shown in Figure 1A). In this screening process, we found that expression of *CLDN18* was abolished in six of eight GC cell lines; however, the other genes listed in Table 1 were expressed in almost all GC cell lines. Thus, we decided to investigate *CLDN18* expression in GC tissues. We next investigated the expression of *CLDN18* in 23 GC tissue samples and 23 corresponding non-neoplastic mucosa samples by quantitative RT-PCR. Of the 23 GC cases, expression of *CLDN18* was down-regulated in 13 (56.5%) (Figure 1B).

Expression of *CLDN18* variant 1 and variant 2 in non-neoplastic tissues and GC tissues

CLDN18 has been reported to have two variants in mice. We first investigated tissue specificity of the expression of *CLDN18* mRNA variants. The conventional RT-PCR primers that we used for the first screening amplified exons 3–5 and this allowed amplification of both variants 1 and 2 (Figure 2). As shown in Figure 2, variant-specific primers were designed. The cDNA of variant 1 was PCR-amplified in normal lung and that of variant 2 was PCR-amplified in normal stomach. The amplified cDNA of each variant was subcloned into pCR2.1. Sequencing analysis confirmed that the inserted PCR fragments obtained from each sample represented each variant, indicating that each variant-specific primer amplified each variant (data not shown). These vectors containing *CLDN18* variant 1 and variant 2 served as positive controls for RT-PCR analysis.

We next investigated *CLDN18* expression in 14 non-neoplastic organs (Figure 3A). *CLDN18* variant 1 was expressed only in normal lung, whereas *CLDN18* variant 2 was expressed in normal stomach and duodenum. Expression of *CLDN18* variant 2 was observed in three of ten GC samples (Figure 3B), whereas the remaining seven samples showed weak or no expression of variant 2. All ten corresponding non-neoplastic gastric mucosa samples expressed *CLDN18* variant 2. *CLDN18* variant 1 was not expressed in any GC or corresponding non-neoplastic mucosa samples. These results indicate that the quantitative RT-PCR data represented *CLDN18* variant 2 and that specifically *CLDN18* variant 2 was down-regulated in GC. In GC cell lines (Figure 3C), expression of *CLDN18* variant 2 was detected in MKN-45 and MKN-74 cell lines. *CLDN18* variant 1 was not expressed in any of the GC cell lines that we studied.

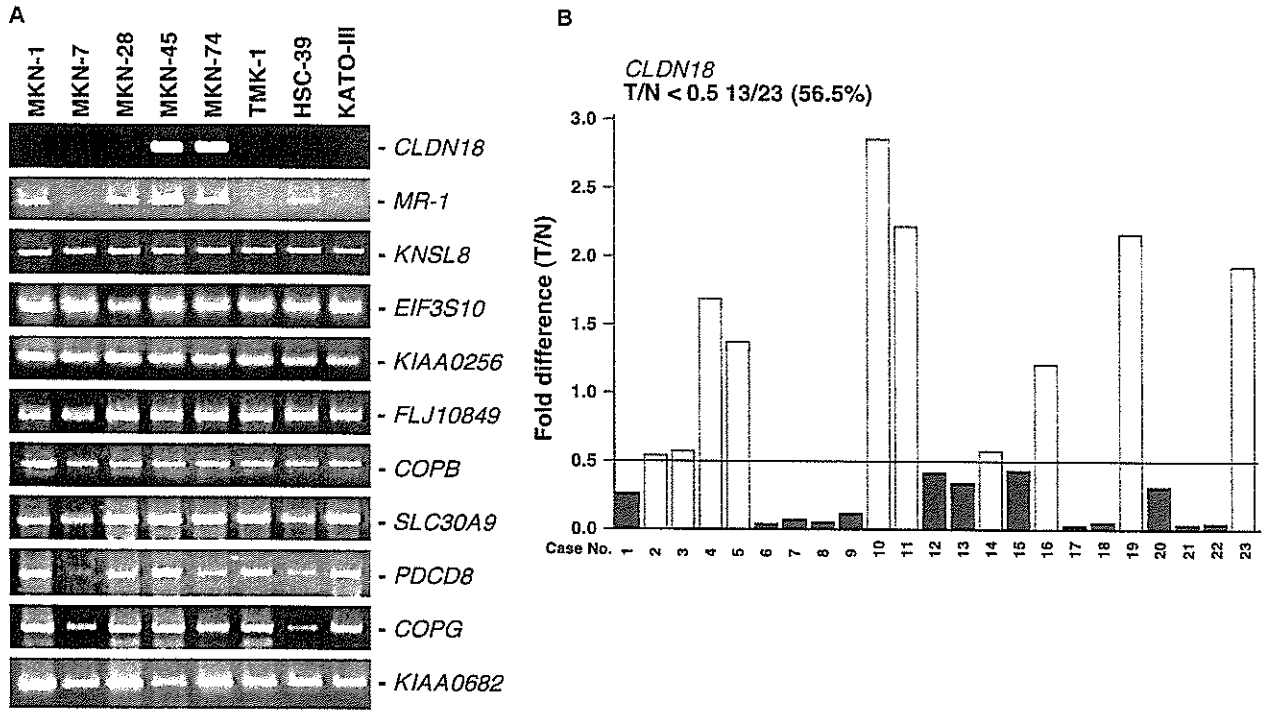

Figure 1. *CLDN18* is down-regulated in GC. (A) Conventional RT-PCR analysis of candidate genes in eight GC cell lines. Expression of *CLDN18* was not detected in six of eight GC cell lines. The remaining genes were expressed frequently. (B) Quantitative RT-PCR analysis of *CLDN18* in GCs and corresponding non-neoplastic mucosa. Fold-change indicates the ratio of *CLDN18* mRNA level in GC (T) to that in corresponding non-neoplastic mucosa (N). Expression of *CLDN18* was reduced (T/N < 0.5) in 13 (56.5%) of 23 GC cases

Expression and localization of claudin-18 in neoplastic and non-neoplastic human tissues

We observed down-regulation of *CLDN18* variant 2 in GC tissues; however, the expression pattern and distribution of claudin-18 protein in GC remain unclear. To address this issue, we performed immunostaining of claudin-18. We first tested the specificity of the anti-claudin-18 antibody. Western blotting of lysates of eight GC cell lines (Figure 3D) was performed and the anti-claudin-18 antibody detected an approximately 29 kD band on western blots of MKN-45 and MKN-74 cell extracts. These results are consistent with the RT-PCR data for *CLDN18* variant 2. The anti-claudin-18 antibody recognizes both claudin-18 variant 1 and variant 2 (Figure 2), but our RT-PCR indicated that only *CLDN18* variant 2 is expressed in GC cell lines, GC, and corresponding non-neoplastic mucosa. Thus, this anti-claudin-18 antibody should recognize only claudin-18 variant 2 in these samples. Immunostaining of GC cell lines revealed that claudin-18 was present in cell membranes of MKN-45 but not MKN-28 cells (Figure 3E). Taken together, these data show that this anti-claudin-18 antibody specifically recognizes claudin-18 protein.

We next performed immunostaining of claudin-18 in non-neoplastic stomach and duodenum because RT-PCR revealed obvious *CLDN18* variant 2 expression in these tissues. In non-neoplastic gastric mucosa, all epithelial cells (foveolar, endocrine, parietal, and chief cells) expressed claudin-18 along the cell membrane but not in the cytoplasm (Figures 4A and 4B). In the duodenum, claudin-18 was expressed in Paneth cells (Figure 4C). Claudin-18 expression was lost in some of the intestinal metaplasia of the stomach (Figure 4D). Stromal cells showed weak or no staining of claudin-18.

In neoplastic lesions, most adenomas (18/20, 90.0%) of the stomach did not express claudin-18. In GC tissues, down-regulation of claudin-18 was observed in both well (Figure 4E) and poorly (Figure 4F) differentiated GC. Some signet ring cell carcinoma cells were positive for claudin-18 (Figure 4G). Membranous immunostaining of claudin-18 was also observed in single GC cells in several poorly differentiated GCs (Figure 4H). Some GCs showed heterogeneity of immunostaining of claudin-18, but a tendency for down-regulation of claudin-18 at the invasive front was not observed. Of 146 GC cases, down-regulation of claudin-18 was observed in 84 (57.5%) cases (0, 63 cases; 1+, 21 cases; 2+, 45 cases; 3+, 17 cases). We analysed the relationship of claudin-18 down-regulation to clinicopathological characteristics. Down-regulation of claudin-18 was not correlated with T grade, N grade, tumour stage, or histological type (Table 3). However, patients with GC showing down-regulation of claudin-18 had a significantly worse survival rate than patients with normal claudin-18 expression ($p = 0.0346$, log-rank test) (Figure 4I).

Claudin-18 is down-regulated in GC with the intestinal phenotype

We further investigated the association between claudin-18 expression and gastric/intestinal phenotype

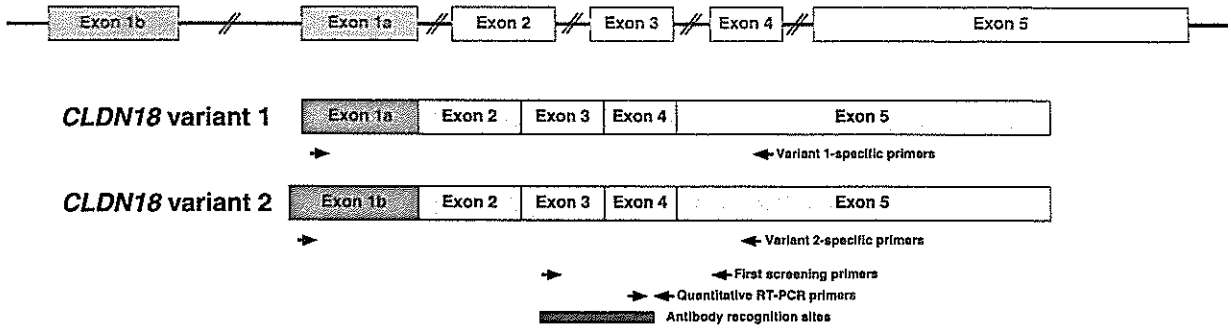

Figure 2. Schematic representation of human *CLDN18* transcript variants. *CLDN18* contains two kinds of exons (exon 1a and exon 1b). Arrows indicate locations of the primers used for RT-PCR analysis. The antibody recognition site is present within the region encoded by exons 3–4

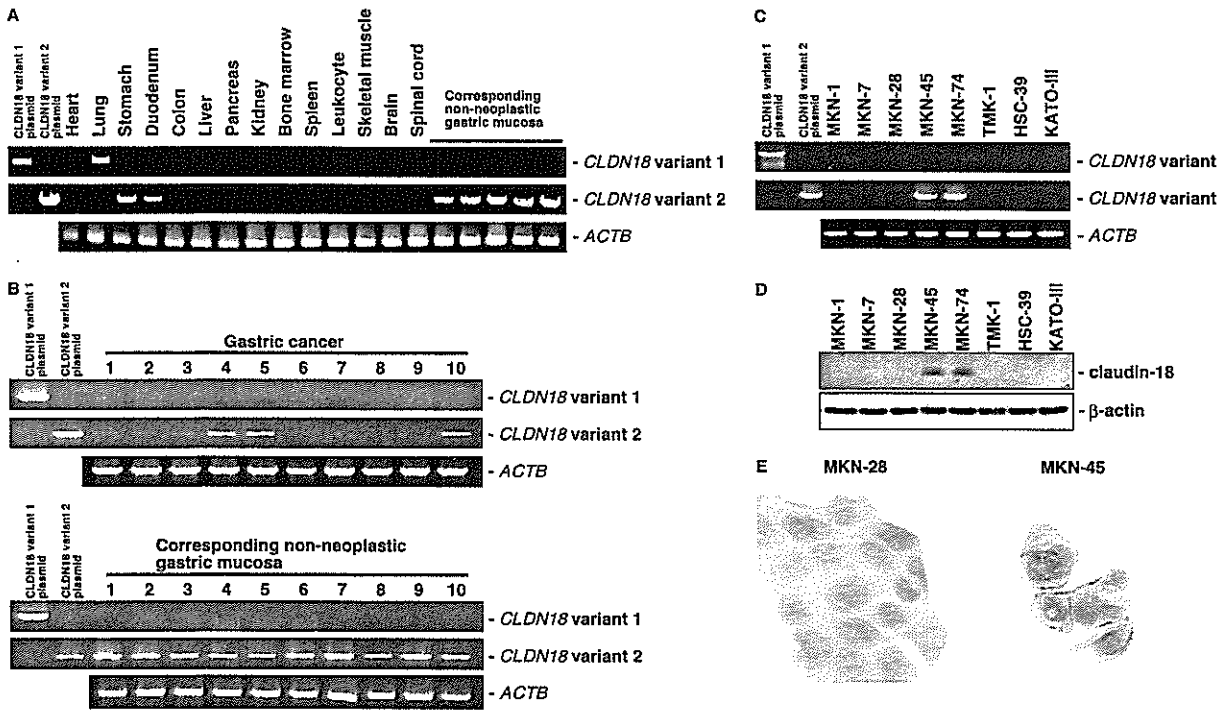

Figure 3. Expression of *CLDN18* variants 1 and 2 in GC tissues and GC cell lines. (A) Conventional RT-PCR analysis of *CLDN18* variants 1 and 2 in 14 non-neoplastic organs. *CLDN18* variant 1 was expressed only in normal lung, whereas *CLDN18* variant 2 was expressed in normal stomach and duodenum. *CLDN18* variant 2 was expressed in all five samples of corresponding non-neoplastic gastric mucosa. Plasmids containing *CLDN18* variant 1 cDNA and *CLDN18* variant 2 cDNA served as positive controls. (B) Conventional RT-PCR analysis of *CLDN18* variants 1 and 2 in GC and corresponding non-neoplastic gastric mucosa. In GC samples, obvious *CLDN18* variant 2 expression was observed in cases 4, 5, and 10. All ten corresponding non-neoplastic gastric mucosa expressed *CLDN18* variant 2. *CLDN18* variant 1 was not expressed in GC and corresponding non-neoplastic mucosa. (C) Conventional RT-PCR analysis of *CLDN18* variants 1 and 2 in GC cell lines. *CLDN18* variant 2 was expressed in MKN-45 and MKN-74 cell lines. (D) Western blot analysis of claudin-18 with anti-claudin-18 antibody. An approximately 29 kD band is present in MKN-45 and MKN-74 cells. (E) Immunostaining of claudin-18 in GC cell lines. In MKN-45 cells, claudin-18 was located to the cell membrane. Claudin-18 was not detected in MKN-28 cells

expression because claudin-18 was down-regulated in intestinal metaplasia of the stomach. Gastric and intestinal markers were detected in 56 of 146 (39.9%) cases for MUC5AC, 12 (8.4%) cases for MUC6, 53 (36.4%) cases for MUC2, and 16 (11.9%) cases for CD10. In some GC cases showing the intestinal phenotype, down-regulation of claudin-18 was observed (Figures 5A–5C), and in several GC cases with the gastric phenotype, claudin-18 expression was detected (Figures 5D–5F). However, even in gastric phenotype GC, claudin-18 was expressed in GC cells that did not express MUC5AC and MUC6 (Figures 5D–5F). In addition, there were several GC cases without the gastric phenotype that showed claudin-18 expression and several GC cases without the intestinal phenotype that did not express claudin-18. In total, there was no clear relationship between expression of claudin-18 and the four gastric/intestinal markers tested (Table 4). On the basis of the expression of these four markers, we classified the 146 GC cases phenotypically as 32 (22.4%) G type, 49 (25.9%) I type, 27 (19.6%) GI

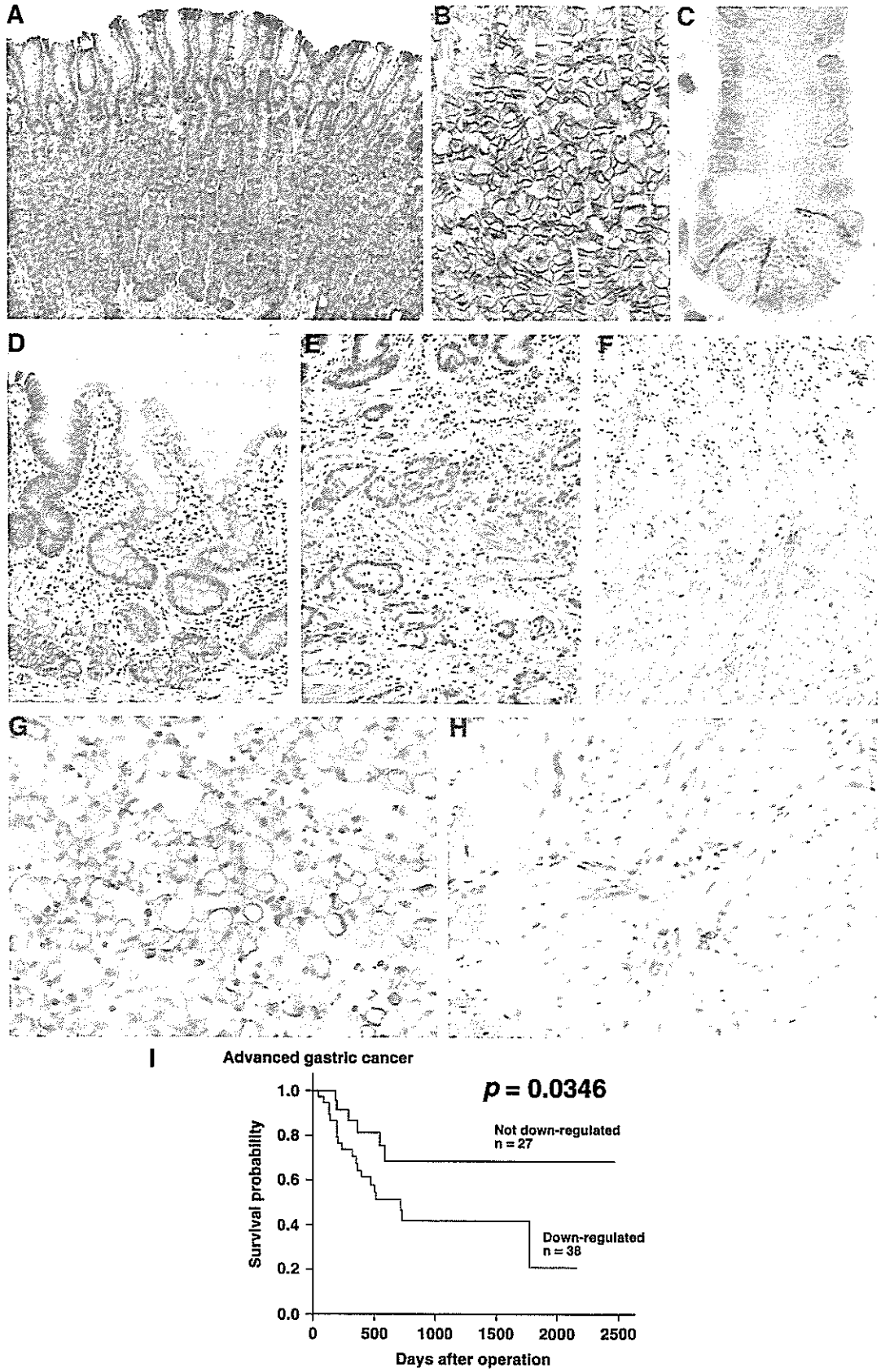

Figure 4. Immunohistochemical analysis of claudin-18 in non-neoplastic stomach and duodenum and in GC tissues. In the stomach (A, B), claudin-18 was detected in all cell membranes. In duodenum (C), only Paneth cells expressed claudin-18. In some intestinal metaplasia of the stomach (D), claudin-18 was not expressed. In GC tissues, down-regulation of claudin-18 was observed in some well (E) and poorly (F) differentiated GCs. Signet ring cell carcinoma cells (G) were positive for claudin-18. Single GC cells in poorly differentiated GC (H) expressed claudin-18. (I) Prognostic value of claudin-18 staining. The survival of patients with GCs showing down-regulation of claudin-18 was significantly worse in the group of 65 patients with advanced GC ($p = 0.0346$, log-rank test). Original magnification: (A) ×100; (B, G, H) ×400; (C) ×1000; (D–F) ×200

type, and 38 (32.2%) N type. Down-regulation of claudin-18 was observed more frequently in I-type GC than in other (G, GI, and N) GC types (Figure 5G).

Discussion

Genes whose expression is down-regulated in cancer may be tumour suppressor genes. Previously, five SAGE studies of GC have been reported, and several up-regulated and down-regulated genes were identified [3,10,17–19]. A combination of SAGE library screening and RT-PCR in the present study revealed that *CLDN18* is down-regulated in GC. Down-regulation of claudin-18 was observed in some intestinal metaplasias and adenomas, suggesting that this change occurs at an early stage of stomach carcinogenesis. GCs are often classified histologically into well and poorly differentiated types on the basis of glandular structure. Several lines of evidence have suggested that intracellular molecules play important roles in histological type-specific carcinogenesis. E-cadherin, a component of adherence junctions, is not expressed in poorly differentiated GCs [20,21]. It has been reported that claudins 1, 3, 4, and 7, and ZO-1, are strongly expressed in most well-differentiated GCs but less frequently in poorly differentiated GCs [19,22]. In the present study, there was no association between claudin-18 expression and histological type. Therefore, down-regulation of claudin-18 is associated with both well and poorly differentiated GC, and it is likely that claudin-18 expression does not participate in glandular differentiation of GC.

In contrast, I-type GC showed frequent down-regulation of claudin-18 in the present study. In fact, *CLDN18* variant 2 was not expressed in the colon, and in the duodenum, claudin-18 was expressed only in Paneth cells. Down-regulation of claudin-18 may be involved in expression of the intestinal phenotype in GC. Expression of the gastric and intestinal phenotypes has been studied mainly according to mucin expression. Several molecules, such as liver-intestine cadherin (Li-cadherin) [23] and regenerating gene type IV (Reg IV) [24], have been reported to be associated with gastric/intestinal phenotype expression in GC. In addition to mucin expression, it appears that other molecules including claudin-18 are likely involved in expression of the gastric and intestinal phenotypes of GC, and give biological behaviour of GC. In the present study, down-regulation of claudin-18 correlated with poor survival, suggesting that down-regulation of claudin-18 may contribute to the malignant behaviour of GC. On the other hand, MUC2 expression has been reported to be associated with a favourable prognosis in GC [25,26]. Similar results have been reported [15]. Because down-regulation of claudin-18 occurred frequently in I-type GC, it is reasonable to speculate that GC showing down-regulation of claudin-18 is associated with favourable survival. However, 17 of 32 G-type GC cases showed down-regulation of claudin-18, indicating that down-regulation of claudin-18 does not occur only in I-type GC and thus, GC showing down-regulation of claudin-18 has several different characteristics from I-type GC.

The biological function of claudin-18 is poorly understood. In addition, little is known about the significance of dysregulation of tight junction proteins in human cancers (discussed in ref 5). The function of the tight junction is maintenance of a luminal barrier, paracellular transport, and signal transduction. Disruption of tight junctions can cause loss of cell polarity, resulting in an abnormal influx of growth factors, which could provide auto- and paracrine stimulation to tumourigenic epithelial cells. Because claudin-18 variant 2 is expressed only in normal stomach and Paneth cells of the duodenum, dysfunction of tight junctions caused by down-regulation of claudin-18 may lead to an abnormal influx of stomach- or Paneth cell-related growth factors. In ovarian cancer, claudin-3 and claudin-4 proteins are highly overexpressed [27] and overexpression of these claudins increases cell invasion and motility [28]. In colon cancer, increased

Table 3. Relationship between claudin-18 protein expression and clinicopathological characteristics in GC

	Claudin-18 expression		
	Down-regulated	Not down-regulated	*p* value*
T grade			
T1	35 (61.4%)	22	0.4950
T2/3/4	49 (55.1%)	40	
N grade			
N0	48 (60.0%)	32	0.6140
N1/2/3	36 (54.5%)	30	
Stage			
I/II	60 (59.4%)	41	0.5870
III/IV	24 (53.3%)	21	
Histology			
Well differentiated	52 (59.8%)	35	0.6090
Poorly differentiated	32 (54.2%)	27	

* Fisher's exact test.

Table 4. Relationship between claudin-18 protein expression and gastric/intestinal markers in GC

	Claudin-18 expression		
	Reduced	Preserved	*p* value*
MUC5AC			
Positive	28 (50.0%)	28	0.1700
Negative	56 (62.2%)	34	
MUC6			
Positive	4 (33.3%)	8	0.1248
Negative	80 (59.7%)	54	
MUC2			
Positive	29 (54.7%)	24	0.6069
Negative	55 (59.1%)	38	
CD10			
Positive	12 (75.0%)	4	0.1821
Negative	72 (55.4%)	58	

* Fisher's exact test.

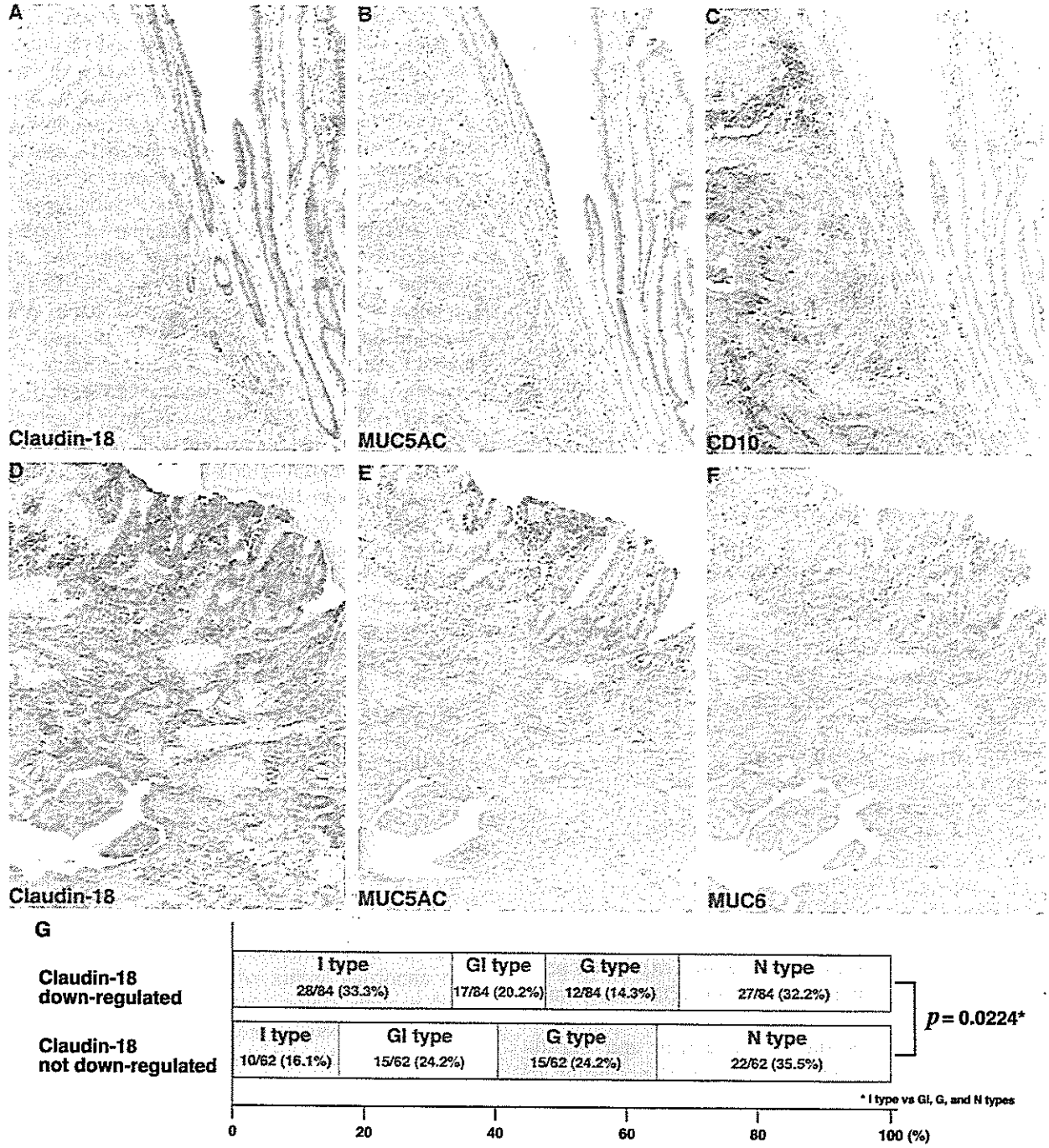

Figure 5. Expression of GC phenotype. In I-type GC (A–C), neither claudin-18 (A) nor MUC5AC (B) was detected by immunohistochemical staining. Expression of CD10 (C) was observed. In G-type GC (D–F), claudin-18 (D) was detected in GC cell membranes. MUC5AC was also expressed in this case, but many claudin-18-positive GC cells did not express MUC5AC (E). MUC6 expression was not found in this case (F). (G) Summary of claudin-18 expression and expression of GC phenotype. Down-regulation of claudin-18 occurred more frequently in I-type GC than in other (GI, G, and N) GC types ($p = 0.0224$, Fisher's exact test). Original magnification: ×100

expression of claudin-1 has been reported and changes in claudin-1 expression have significant effects on the growth of xenografted tumours and metastasis in athymic mice [29].

Whether the *CLDN18* gene is a tumour suppressor or not remains to be determined. It has been reported that Sox2, an HMG-box gastric transcription factor, may play an important role in maintaining the gastric phenotype in GC as well as normal stomach [30,31]. Thus, Sox2 may induce *CLDN18* variant 2 expression.

In the present study, we investigated only *CLDN18* gene expression in GC tissue samples: the remaining genes listed in Table 1 were not investigated in these samples because these genes were expressed in almost all GC cell lines. Further studies of these genes should be performed in the near future.

In summary, our data show that expression of *CLDN18* variant 2 is down-regulated in GC and that this reduced expression correlates with poor survival in patients with GC. Because claudin-18 is frequently

down-regulated in I-type GC, loss of claudin-18 may be a key factor mediating the biological behaviour of I-type GC.

Acknowledgements

We thank M Takatani for excellent technical assistance and advice. This work was carried out with the kind cooperation of the Research Center for Molecular Medicine, Faculty of Medicine, Hiroshima University. We thank the Analysis Center of Life Science, Hiroshima University for the use of their facilities. This work was supported, in part, by Grants-in-Aid for Cancer Research from the Ministry of Education, Culture, Science, Sports, and Technology of Japan; and from the Ministry of Health, Labour, and Welfare of Japan.

References

1. Yasui W, Yokozaki H, Fujimoto J, Naka K, Kuniyasu H, Tahara E. Genetic and epigenetic alterations in multistep carcinogenesis of the stomach. *J Gastroenterol* 2000;**35:**111–115.
2. Ushijima T, Sasako M. Focus on gastric cancer. *Cancer Cell* 2004;**5:**121–125.
3. Oue N, Hamai Y, Mitani Y, Matsumura S, Oshimo Y, Aung PP, *et al.* Gene expression profile of gastric carcinoma: identification of genes and tags potentially involved in invasion, metastasis, and carcinogenesis by serial analysis of gene expression. *Cancer Res* 2004;**64:**2397–2405.
4. Tsukita S, Furuse M, Itoh M. Multifunctional strands in tight junctions. *Nature Rev Mol Cell Biol* 2001;**2:**285–293.
5. Swisshelm K, Macek R, Kubbies M. Role of claudins in tumorigenesis. *Adv Drug Deliv Rev* 2005;**57:**919–928.
6. Niimi T, Nagashima K, Ward JM, Minoo P, Zimonjic DB, Popescu NC, *et al.* Claudin-18, a novel downstream target gene for the T/EBP/NKX2.1 homeodomain transcription factor, encodes lung- and stomach-specific isoforms through alternative splicing. *Mol Cell Biol* 2001;**21:**7380–7390.
7. Ochiai A, Yasui W, Tahara E. Growth-promoting effect of gastrin on human gastric carcinoma cell line TMK-1. *Jpn J Cancer Res* 1985;**76:**1064–1071.
8. Yanagihara K, Seyama T, Tsumuraya M, Kamada N, Yokoro K. Establishment and characterization of human signet ring cell gastric carcinoma cell lines with amplification of the c-myc oncogene. *Cancer Res* 1991;**51:**381–386.
9. Sobin LH, Wittekind CH (eds). *TNM Classification of Malignant Tumors* (6th edn). Wiley-Liss: New York, 2002; 65–68.
10. El-Rifai W, Moskaluk CA, Abdrabbo MK, Harper J, Yoshida C, Riggins GJ, *et al.* Gastric cancers overexpress S100A calcium-binding proteins. *Cancer Res* 2002;**62:**6823–6826.
11. Lal A, Lash AE, Altschul SF, Velculescu V, Zhang L, McLendon RE, *et al.* A public database for gene expression in human cancers. *Cancer Res* 1999;**59:**5403–5407.
12. Gibson UE, Heid CA, Williams PM. A novel method for real time quantitative RT-PCR. *Genome Res* 1996;**6:**995–1001.
13. Kondo T, Oue N, Yoshida K, Mitani Y, Naka K, Nakayama H, *et al.* Expression of POT1 is associated with tumor stage and telomere length in gastric carcinoma. *Cancer Res* 2004;**64:**523–529.
14. Yasui W, Ayhan A, Kitadai Y, Nishimura K, Yokozaki H, Ito H, *et al.* Increased expression of p34cdc2 and its kinase activity in human gastric and colonic carcinomas. *Int J Cancer* 1993;**53:**36–41.
15. Mizoshita T, Tsukamoto T, Nakanishi H, Inada K, Ogasawara N, Joh T, *et al.* Expression of Cdx2 and the phenotype of advanced gastric cancers: relationship with prognosis. *J Cancer Res Clin Oncol* 2003;**129:**727–734.
16. Mantel N. Evaluation of survival data and two new rank order statistics arising in its consideration. *Cancer Chemother Rep* 1966;**50:**163–170.
17. Oien KA, Vass JK, Downie I, Fullarton G, Keith WN. Profiling, comparison and validation of gene expression in gastric carcinoma and normal stomach. *Oncogene* 2003;**22:**4287–4300.
18. Lee JY, Eom EM, Kim DS, Ha-Lee YM, Lee DH. Analysis of gene expression profiles of gastric normal and cancer tissues by SAGE. *Genomics* 2003;**82:**78–85.
19. Johnson AH, Frierson HF, Zaika A, Powell SM, Roche J, Crowe S, *et al.* Expression of tight-junction protein claudin-7 is an early event in gastric tumorigenesis. *Am J Pathol* 2005;**167:**577–584.
20. Shimoyama Y, Hirohashi S. Expression of E- and P-cadherin in gastric carcinomas. *Cancer Res* 1991;**51:**2185–2192.
21. Oue N, Motoshita J, Yokozaki H, Hayashi K, Tahara E, Taniyama K, *et al.* Distinct promoter hypermethylation of p16INK4A, CDH1, and RAR-beta in intestinal, diffuse-adherent, and diffuse-scattered-type gastric carcinomas. *J Pathol* 2002;**198:**55–59.
22. Resnick MB, Gavilanez M, Newton E, Konkin T, Bhattacharya B, Britt DE, *et al.* Claudin expression in gastric adenocarcinomas: a tissue microarray study with prognostic correlation. *Hum Pathol* 2005;**36:**886–892.
23. Ito R, Oue N, Yoshida K, Kunimitsu K, Nakayama H, Nakachi K, *et al.* Clinicopathological significant and prognostic influence of cadherin-17 expression in gastric cancer. *Virchows Arch* 2005;**447:**717–722.
24. Oue N, Mitani Y, Aung PP, Sakakura C, Takeshima Y, Kaneko M, *et al.* Expression and localization of Reg IV in human neoplastic and non-neoplastic tissues: Reg IV expression is associated with intestinal and neuroendocrine differentiation in gastric adenocarcinoma. *J Pathol* 2005;**207:**185–198.
25. Utsunomiya T, Yonezawa S, Sakamoto H, Kitamura H, Hokita S, Aiko T, *et al.* Expression of MUC1 and MUC2 mucins in gastric carcinomas: its relationship with the prognosis of the patients. *Clin Cancer Res* 1998;**4:**2605–2614.
26. Baldus SE, Zirbes TK, Engel S, Hanisch FG, Monig SP, Lorenzen J, *et al.* Correlation of the immunohistochemical reactivity of mucin peptide cores MUC1 and MUC2 with the histopathological subtype and prognosis of gastric carcinomas. *Int J Cancer* 1998;**79:**133–138.
27. Hough CD, Sherman-Baust CA, Pizer ES, Montz FJ, Im DD, Rosenshein NB, *et al.* Large-scale serial analysis of gene expression reveals genes differentially expressed in ovarian cancer. *Cancer Res* 2000;**60:**6281–6287.
28. Agarwal R, D'Souza T, Morin PJ. Claudin-3 and claudin-4 expression in ovarian epithelial cells enhances invasion and is associated with increased matrix metalloproteinase-2 activity. *Cancer Res* 2005;**65:**7378–7385.
29. Dhawan P, Singh AB, Deane NG, No Y, Shiou SR, Schmidt C, *et al.* Claudin-1 regulates cellular transformation and metastatic behavior in colon cancer. *J Clin Invest* 2005;**115:**1765–1776.
30. Tatematsu M, Tsukamoto T, Inada K. Stem cells and gastric cancer: role of gastric and intestinal mixed intestinal metaplasia. *Cancer Sci* 2003;**94:**135–141.
31. Tsukamoto T, Mizoshita T, Mihara M, Tanaka H, Takenaka Y, Yamamura Y, *et al.* Sox2 expression in human stomach adenocarcinomas with gastric and gastric-and-intestinal-mixed phenotypes. *Histopathology* 2005;**46:**649–658.

MOLECULAR AND CELLULAR BIOLOGY, Feb. 2006, p. 898–911 Vol. 26, No. 3
0270-7306/06/$08.00+0 doi:10.1128/MCB.26.3.898–911.2006
Copyright © 2006, American Society for Microbiology. All Rights Reserved.

Glycogen Synthase Kinase 3 and h-prune Regulate Cell Migration by Modulating Focal Adhesions†

Tsuyoshi Kobayashi,[1,2] Shin-ichiro Hino,[1] Naohide Oue,[3] Toshimasa Asahara,[2] Massimo Zollo,[4] Wataru Yasui,[3] and Akira Kikuchi[1]*

Departments of Biochemistry,[1] Surgery,[2] and Molecular Pathology,[3] Graduate School of Biomedical Sciences, Hiroshima University, Hiroshima, Japan, and CEINGE, Biotecnologie Avanzate s.c.ar.l., Napoli, Italy[4]

Received 25 July 2005/Returned for modification 2 September 2005/Accepted 4 November 2005

h-prune, which has been suggested to be involved in cell migration, was identified as a glycogen synthase kinase 3 (GSK-3)-binding protein. Treatment of cultured cells with GSK-3 inhibitors or small interfering RNA (siRNA) for GSK-3 and h-prune inhibited their motility. The kinase activity of GSK-3 was required for the interaction of GSK-3 with h-prune. h-prune was localized to focal adhesions, and the siRNA for GSK-3 or h-prune delayed the disassembly of paxillin. The tyrosine phosphorylation of focal adhesion kinase (FAK) and the activation of Rac were suppressed in GSK-3 or h-prune knocked-down cells. GSK-3 inhibitors suppressed the disassembly of paxillin and the activation of FAK and Rac. Furthermore, h-prune was highly expressed in colorectal and pancreatic cancers, and the positivity of the h-prune expression was correlated with tumor invasion. These results suggest that GSK-3 and h-prune cooperatively regulate the disassembly of focal adhesions to promote cell migration and that h-prune is useful as a marker for tumor aggressiveness.

The serine/threonine kinase glycogen synthase kinase 3 (GSK-3) was first described for a metabolic pathway for glycogen synthase regulation that is sensitive to insulin-mediated inhibition (35). GSK-3 has subsequently been shown to regulate several physiological responses, including protein synthesis, gene expression, subcellular localization of proteins, and protein degradation, in mammalian cells by phosphorylating many substrates (5, 9, 16). There are two members of GSK-3α and GSK-3β in mammals (49). GSK-3 is highly conserved through evolution and plays a fundamental role in cellular responses. For example, there are four genes, *MCK1*, *MDS1/RIM11*, *MRK1*, and *YOL128c*, which encode homologs of mammalian GSK-3 in *Saccharomyces cerevisiae*. Mck1 stabilizes Rog1 (1) and stimulates gene expression by Msn2 in yeasts (19).

To understand the molecular mechanism by which GSK-3 recognizes specific target substrates, we have tried to isolate proteins that bind to GSK-3. So far, we have identified Axin, Axil, and AKAP220 as GSK-3β-binding proteins (21, 43, 52). Axin binds to not only GSK-3 but also β-catenin, APC, and Dvl, all of which are important components in the Wnt signaling pathway (25, 48). In the Axin complex, GSK-3 phosphorylates β-catenin, APC, and Axin efficiently (21, 27) and thereby induces ubiquitination of β-catenin, leading to its degradation. Axil has characteristics similar to those of Axin (52). AKAP220 binds to not only GSK-3 but also cyclic AMP (cAMP)-dependent protein kinase and protein phosphatase 1 (43). The phosphorylation and dephosphorylation of GSK-3 occur efficiently in the AKAP220 complex. Therefore, GSK-3 may exhibit different functions and regulation depending on its binding partners.

Evidence that GSK-3 regulates cellular architecture in neuronal cells has been accumulated (5, 24). Two microtubule-associating proteins, Tau and MAP1B, are phosphorylated by GSK-3, which regulates their binding to microtubules, thereby modulating microtubule dynamics. An inactive pool of GSK-3 has been found to be localized at the leading edge of the cells alongside F-actin, and semapholin 3A and lysophosphatidic acid activate GSK-3, causing growth cone collapse and neurite retraction (10). GSK-3 mediates Par6-PKCζ-dependent promotion of polarization and cell protrusion in astrocytes (11). Furthermore, GSK-3 phosphorylates CRMP2 to specify the fate of axons and dendrites (54). GSK-3 has also been shown to be involved in signaling activated by cell adhesion in nonneuronal cells (23, 37). The formation of extending lamellipodia in migrating keratinocytes is blocked by GSK-3 inhibitors (29). The initiation and stimulation of sperm motility are accompanied by the inactivation of GSK-3 (41). Although these results suggest that GSK-3 is involved in the dynamics of actin filaments and microtubules, how the GSK-3 activity is linked to molecules involved in cell migration is not clearly understood.

The human homolog of *Drosophila* prune protein (h-prune) belongs to the DHH superfamily of phosphodiesterases (PDE), which have cytoplasmic cyclic nucleotide phosphodiesterase activity (8). Overexpression of h-prune in cultured cells is involved in promoting cellular motility, and inhibition of PDE activity by a PDE inhibitor suppresses h-prune-induced motility (8). Consistent with these observations, overexpression of h-prune in breast cancer is correlated with cancer progression and aggressiveness (55). However, the molecular mechanism by which h-prune regulates cell motility remains to be defined.

To understand the molecular mechanism by which GSK-3 regulates cell migration, we screened new GSK-3-binding proteins. Here, we identified h-prune as a GSK-3-binding protein.

* Corresponding author. Mailing address: Department of Biochemistry, Graduate School of Biomedical Sciences, Hiroshima University, 1-2-3 Kasumi, Minami-ku, Hiroshima 734-8551, Japan. Phone: 81-82-257-5130. Fax: 81-82-257-5134. E-mail: akikuchi@hiroshima-u.ac.jp.

† Supplemental material for this article may be found at http://mcb.asm.org/.

Knockdown of GSK-3 and h-prune by small interfering RNA (siRNA) suppressed cell migration. h-prune formed a complex with paxillin and vinculin at focal adhesions. Loss of activity of GSK-3 or knockdown of GSK-3 and h-prune inhibited the disassembly of paxillin, the tyrosine phosphorylation of focal adhesion kinase (FAK), and the activation of Rac. These results indicate that GSK-3 and h-prune cooperatively regulate the disassembly of focal adhesions to regulate cell migration.

MATERIALS AND METHODS

Materials and chemicals. HeLa S3 and C57MG cells were provided by K. Matsumoto (Nagoya University, Nagoya, Japan) and S. Takada (National Institutes of Natural Sciences, Okazaki, Japan), respectively. Human GSK-3β cDNA was provided by J. R. Woodgett (Ontario Cancer Institute, Toronto, Canada). Recombinant baculoviruses expressing glutathione *S*-transferase (GST)-fused h-prune wild type (WT) were generated by Y. Matsuura (Osaka University, Suita, Japan). Paxillin cDNA and pGEX-αPAK-CRIB were provided by H. Sabe (Osaka Bioscience Institute, Osaka, Japan) and K. Kaibuchi (Nagoya University, Nagoya, Japan), respectively. Green fluorescent protein (GFP)-tagged Super-FAK (the K578E/K581E mutant) was provided by M. D. Schaller (University of North Carolina, Chapel Hill, NC) (15). HeLa S3 cells stably expressing h-prune (WT) or amino acid region 199 to 453 of h-prune [h-prune(199-453)] were generated by selection with G418. NIH 3T3 and HeLa S3 cells stably expressing GFP-paxillin were generated by selection with puromycin. The anti-Myc antibody was prepared from 9E10 cells. The anti-h-prune antibody was prepared in rabbits by immunization with recombinant h-prune(199-453) proteins. siRNA duplexes used were as follows: human GSK-3α (sense), 5′-GAAGGUUCUCC AGGACAAGTT-3′; human GSK-3β (sense), 5′-AGUUAGCAGAGACAAGG ACTT-3′; mouse GSK-3β (sense), 5′-GAAGUCUAGCCUAUAUCCATT-3′; h-prune (sense), 5′-GGCGUCAAGGUGGCCAUUATT-3′; and human casein kinase Iα (CKIα) (sense), 5′-CCAGGCAUCCCCAGUUGCUTT-3′. Other materials were from commercial sources.

Plasmid construction. pCGN/GSK-3β (WT), pCGN/GSK-3β K85M, pCGN/GSK-3β K85R, pCGN/GSK-3β Y216F, pCGN/GSK-3β S9A, and pGEX-4T/GSK-3β (WT) were constructed as previously described (21, 43). Standard recombinant DNA techniques were used to construct the following plasmids: pEF-BOS-Myc/h-prune (WT), pEF-BOS-Myc/h-prune(1-332), pEF-BOS-Myc/h-prune(199-453), pEF-BOS-Myc/h-prune(333-453), pGEX-6P/h-prune (WT), pV-IKS/h-prune (WT), pAd-CMV-Myc/h-prune (WT), and pRSETA/GSK-3β (WT).

Cell culture. COS, NIH 3T3, and HeLa S3 cells were grown in Dulbecco's modified Eagle's medium supplemented with 10% calf serum and 10% fetal bovine serum (FBS). C57MG cells were grown in Dulbecco's modified Eagle's medium supplemented with 10% FBS and 10 μg/ml insulin. SW480 and CHO cells were grown in RPMI medium and Ham's F-12 medium supplemented with 10% FBS, respectively. When necessary, the cells were treated with 3 to 10 μM SB216763 for 4 h or 10 to 30 mM LiCl for 12 h or transfected with the siRNA for GSK-3β or h-prune.

Cell migration assay. To measure the cell migration activity, Transwell and wound-healing assays were performed. The Transwell cell migration assay was performed using a modified Boyden chamber (tissue culture treated, 6.5-mm diameter, 10-μm thickness, 8-μm pores; Transwell) (Costar, Cambridge, MA) as described previously (20, 32). The haptotactic migration assay was done by coating only the lower surface of the polycarbonate membrane with 10 μg/ml collagen or fibronectin, whereas the random migration assay was done by coating both the upper and lower surfaces of the membrane with 0.1 μg/ml collagen. HeLa S3, SW480, and CHO cells (2.5×10^4 cells) and NIH 3T3 cells (2.5×10^5 cells) suspended in serum-free medium containing 0.1% bovine serum albumin with or without inhibitors were applied to the upper chamber and allowed to migrate to the lower side of the upper chamber for 2 to 12 h. The numbers of the cells that migrated to the lower side of the upper chamber were counted, and relative cell migration was expressed as the percentage of migrated cells with treatment compared to those without treatment.

To carry out the wound-healing assay, HeLa S3, C57MG, NIH 3T3, and SW480 cells were plated onto collagen- or fibronectin-coated coverslips. The monolayer cells were then scratched manually with a plastic pipette tip, and after being washed with phosphate-buffered saline, wounded monolayers of the cells were allowed to heal for 12 to 24 h.

Immunohistochemistry. The immunocytochemical analyses of the cultured cells were performed as described previously (51) except that the cultured cells were simultaneously fixed and permeabilized with phosphate-buffered saline containing 3.7% paraformaldehyde and 0.5% Triton X-100. The immunohistochemical analyses of paraffin-embedded tissues from patients were performed as previously described (30). The sections were counterstained with 0.1% hematoxylin. A result was considered positive when more than 50% of the cells were stained.

Clinicopathological analyses of h-prune. For immunohistochemical analyses, we used archival formalin-fixed, paraffin-embedded tissues from 134 patients who had undergone surgical excision for colorectal cancer (adenocarcinoma) (n = 92) or pancreatic cancer (ductal adenocarcinoma) (n = 42). Tumor staging was carried out according to the TNM staging system (40). The procedure to protect privacy was in accordance with the Ethical Guidelines for Human Genome/Gene Research enacted by the Japanese government. Correlations between clinicopathologic parameters and h-prune expression were analyzed by Fisher's exact test. P values less than 0.05 were considered statistically significant.

Live imaging of adhesion and lamellipodia. The dynamics of GFP-paxillin of the scratched monolayer cells were quantified as described previously (14, 46). Fluorescence intensities of individual adhesions from background-subtracted images were measured over time using MetaMorph software (Universal Imaging Corporation, Downingtown, PA). For rate constant measurements, periods of disassembly (decreasing fluorescence intensity) of adhesions containing GFP-paxillin were plotted on separate semilogarithmic graphs representing fluorescence intensity ratios over time. Semilogarithmic plots of fluorescence intensities as a function of time were generated using the formula $\ln (I_0/I)$ for disassembly, where I_0 is the initial fluorescence intensity and I is the fluorescence intensity at various time points. The slopes of linear regression trend lines fitted to the semilogarithmic plots were then calculated to determine apparent rate constants of disassembly. For each rate constant, measurements were made on at least 10 individual adhesions in five separate cells. For lamellipodium formation, images were captured at 5-min intervals for 60 min. The average area of protrusion (μm^2) per 5-min interval was calculated. Measurements were made with at least five separate cells (7).

Others. Yeast two-hybrid screening was carried out as previously described (21, 52). Immunoprecipitation assays and RNA interference (RNAi) were performed as described previously (18, 51). The GSK-3 activity was assayed by the use of synthetic peptides as substrates (21, 43). The PDE activity of HeLa S3 cells was assayed using [^{3}H]cAMP as a substrate (44). Activation of Rac was assayed using GST-CRIB (2).

RESULTS

Involvement of GSK-3 in cell migration. First, we examined the involvement of GSK-3 in cell motility using a Transwell migration assay. HeLa S3 cells migrated over both collagen and fibronectin (Fig. 1A). LiCl, which is known to inhibit GSK-3 activity (28, 42), reduced the migration of HeLa S3 cells, but NaCl did not affect the migration (Fig. 1A). SB216763, which is another GSK-3 inhibitor, also suppressed the migration (Fig. 1A). CHO cells migrated over fibronectin but not collagen, and LiCl reduced the migration (Fig. 1B). Overexpression of wild-type GSK-3β or a constitutively active form of GSK-3β did not affect cell migration (data not shown), indicating that GSK-3 is not a limiting factor for migration.

We depleted endogenous GSK-3 in HeLa S3 cells by RNAi to find whether GSK-3 is definitively involved in the regulation of cell migration. An siRNA for GSK-3β or GSK-3α reduced the respective levels but not the levels of vinculin and CKIα (Fig. 1C). A single-stranded sense oligonucleotide for GSK-3β or siRNA for CKIα did not affect the protein levels of GSK-3β and GSK-3α (Fig. 1C). A decrease of either GSK-3β or GSK-3α but not CKIα inhibited the migration of HeLa S3 cells (Fig. 1C). Since these assays were done by coating the lower surface of the membranes with substrates, these results indicate the involvement of GSK-3 in haptotaxis. Random migration was measured by coating both the upper and lower surfaces of the membrane with the substrates. Inhibition of GSK-3 also suppressed the random migration of HeLa S3 cells

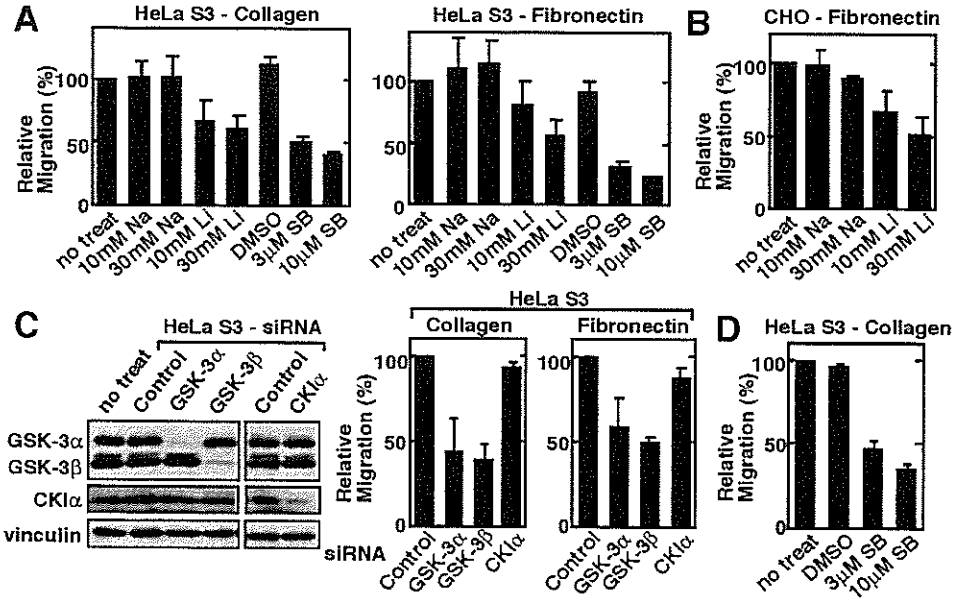

FIG. 1. Involvement of GSK-3 in cell migration. (A) HeLa S3 cells treated with the indicated inhibitors were subjected to the Transwell migration assay. (B) CHO cells treated with NaCl or LiCl were subjected to the Transwell migration assay. (C) Left panel, the lysates of HeLa S3 cells transfected with the indicated siRNAs were probed with the indicated antibodies. Right panel, HeLa S3 cells transfected with the indicated siRNAs were subjected to the Transwell migration assay. A single-strand RNA for GSK-3β was used as a control. (D) HeLa S3 cells treated with SB216763 were subjected to the random migration assay. The results shown are means ± standard errors of the means from four independent experiments. DMSO, dimethyl sulfoxide; Na, NaCl; Li, LiCl; SB, SB216763; no treat, no treatment.

(Fig. 1D). Therefore, GSK-3 is involved in both haptotactic and random migration. In the following experiments, we used a haptotactic assay. Inhibition of GSK-3 by LiCl in CHO cells and reduction of GSK-3β by RNAi in HeLa S3 cells did not inhibit cell adhesiveness (data not shown).

Identification of h-prune as a GSK-3-binding protein. To identify GSK-3-binding proteins that are involved in cell migration, we screened a human brain cDNA library using the yeast two-hybrid method. A 1.8-kb cDNA insert was found to carry a sequence containing an open reading frame for h-prune (Fig. 2A). h-prune belongs to the DHH family and exhibits PDE activity, and overexpression of h-prune enhances cell migration, which is inhibited by the suppression of its PDE activity (8).

Reciprocal immunoprecipitation analyses showed that GSK-3β and h-prune formed a complex at the endogenous level in HeLa S3 cells (Fig. 2B). GSK-3α also formed a complex with h-prune (Fig. 2B). In vitro binding studies using recombinant proteins demonstrated that GSK-3β bound directly to h-prune (Fig. 2C). Amino acid region 333 to 453 of h-prune was necessary and sufficient for the complex formation with GSK-3β in intact cells (Fig. 2D). Treatment of HeLa S3 cells with GSK-3 inhibitors decreased the formation of a complex between GSK-3β and h-prune (Fig. 2E). Furthermore, GSK-3β kinase-inactive mutants (the K85M, K85R, and Y216F mutants) did not form a complex with h-prune under the conditions in which wild-type GSK-3β and a constitutively active GSK-3β mutant (S9A) did (Fig. 2F). These results indicate that the kinase activity of GSK-3 is required for its interaction with h-prune in intact cells. GSK-3 did not phosphorylate h-prune in vitro, and SB216763 did not affect the phosphorylation of h-prune in intact cells, where ^{32}P was metabolically labeled (data not shown). h-prune does not possess the typical consensus sequences for phosphorylation by GSK-3. Therefore, it is unlikely that h-prune is a substrate of GSK-3.

The kinase activity of GSK-3 in the h-prune immune com-

FIG. 2. Interaction of h-prune with GSK-3. (A) Schematic representation of the deletion mutants of h-prune used in this study. (B) The lysates of HeLa S3 cells (lanes 1 and 6) were immunoprecipitated with anti-GSK-3β or anti-h-prune antibody, and the immunoprecipitates were probed with the indicated antibodies (lanes 3, 5, and 8). The immunoprecipitates formed with anti-Myc and anti-GFP antibodies were used as controls (lanes 2, 4, and 7). GSK-3α/β Ab is an antibody that recognizes both GSK-3α (α) and GSK-3β (β). (C) Recombinant His_6-GSK-3β, GST-h-prune, and GST (0.5 μg of protein) were stained with Coomassie brilliant blue (lanes 1 to 3). After 0.4 μM His_6-GSK-3β was incubated with 0.5 μM GST-h-prune or GST immobilized on glutathione-Sepharose in 100 μl of reaction mixture (20 mM Tris/HCl, pH 7.5, and 1 mM dithiothreitol) for 1 h at 4°C, GST-h-prune and GST were precipitated by centrifugation, and then the precipitates were probed with the anti-His_6 antibody (lanes 4 to 6). (D) The lysates of COS cells expressing the deletion mutants of Myc-h-prune were probed with anti-GSK-3β or anti-Myc antibody (lanes 1 to 5). The same lysates were immunoprecipitated with anti-Myc antibody, and the immunoprecipitates were probed with the indicated antibodies (lanes 6 to 10). (E) HeLa S3 cells treated with 10 μM SB216763 or 30 mM LiCl were lysed, and the lysates were probed with anti-GSK-3β or anti-h-prune antibody (lanes 1 to 4). The same lysates were immunoprecipitated with anti-GSK-3β (lanes 5 to 6) or anti-h-prune antibody (lanes 7 to 10), and the immunoprecipitates were probed with the indicated antibodies. The lower bands detected by anti-h-prune antibody in Fig. 2B

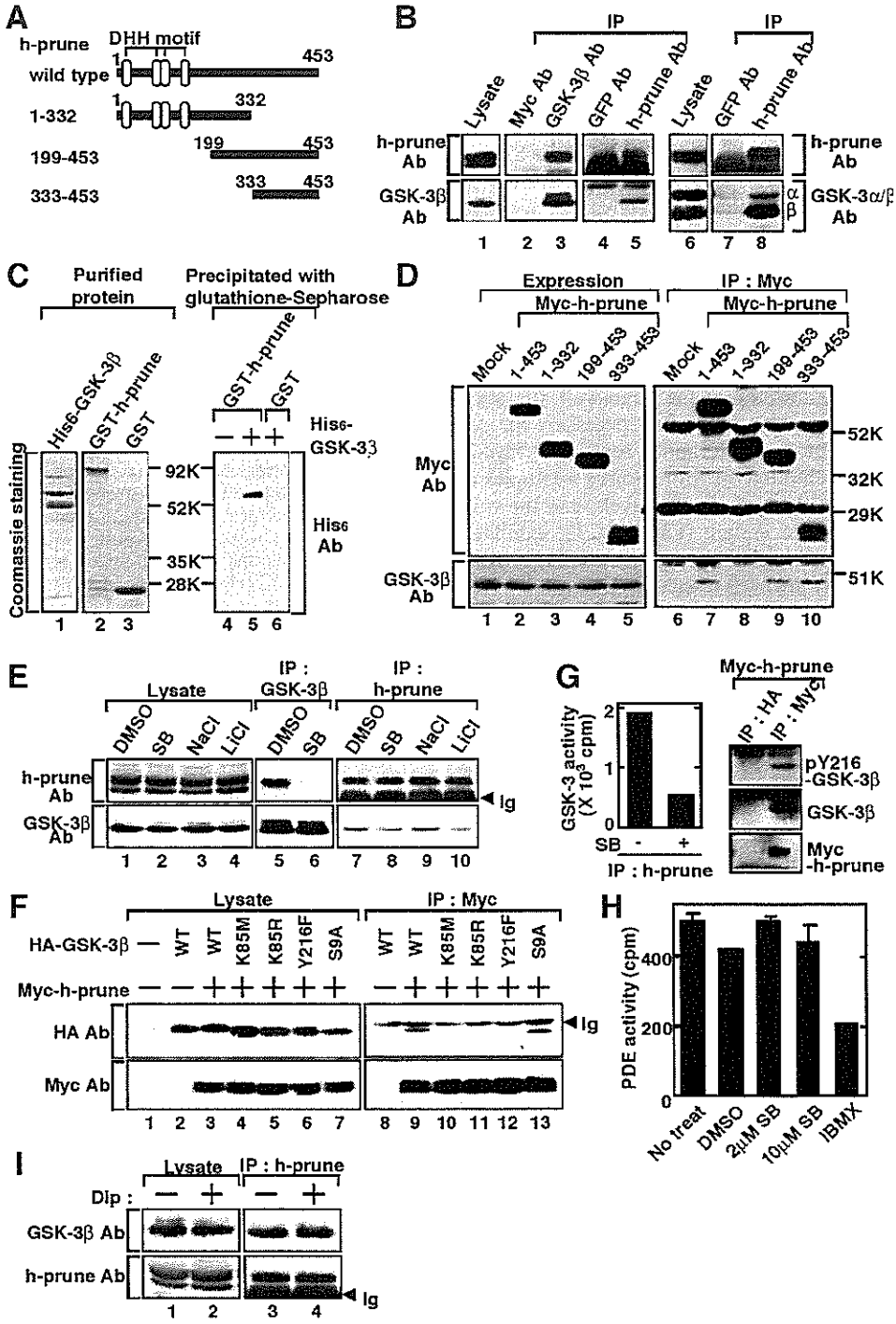

and E are nonspecific bands. (F) The lysates of COS cells expressing HA–GSK-3β mutants and Myc-h-prune were probed with anti-HA or anti-Myc antibody (lanes 1 to 7). The same lysates were immunoprecipitated with anti-Myc antibody, and the immunoprecipitates were probed with the indicated antibodies (lanes 8 to 13). (G) Left panel, the kinase activity of GSK-3 in the immunoprecipitates from HeLa S3 cells with anti-h-prune antibody was measured in the presence or absence of SB216763 in vitro. Right panel, the lysates of HeLa S3 cells expressing Myc-h-prune were immunoprecipitated with anti-Myc or anti-HA antibody, and the immunoprecipitates were probed with anti-GSK-3β antibody and the phospho-specific antibody to GSK-3β Tyr216 (pY216-GSK-3β). (H) The PDE activity of h-prune in HeLa S3 cells was measured after treatment with SB216763 in intact cells or with IBMX in vitro. (I) After HeLa S3 cells were treated with 10 μM dipyridamole for 4 h, h-prune was immunoprecipitated from the lysates and the immunoprecipitates were probed with anti-GSK-3β and anti-h-prune antibodies. HA, hemagglutinin; IP, immunoprecipitation; Ab, antibody; SB, SB216763; Dip, dipyridamole; Ig, immunoglobulin; DMSO, dimethyl sulfoxide; no treat, no treatment; Mock, control.

plexes was detected using peptide substrates, and the Tyr216-phosphorylated form of GSK-3β, which is an active form, was observed in the h-prune immune complexes (Fig. 2G), indicating that GSK-3 complexed with h-prune is active. The PDE activity in the h-prune immune complexes from HeLa S3 cells expressing h-prune was measured using [^{3}H]cAMP as a substrate. This activity was indeed inhibited by 3-isobutyl-1-methylxanthine (IBMX), a well-known PDE inhibitor. However, the PDE activity was not affected by the treatment of HeLa S3 cells with GSK-3 inhibitors (Fig. 2H). Therefore, the kinase activity of GSK-3 is not required for the PDE activity of h-prune. Dipyridamole was shown to inhibit the PDE activity (8). Treatment of HeLa S3 cells with dipyridamole did not affect the complex formation between h-prune and GSK-3β (Fig. 2I), suggesting that the PDE activity of h-prune is not necessary for the binding of h-prune to GSK-3.

Involvement of h-prune in cell migration. An siRNA for h-prune suppressed cell motility in the Transwell migration assay (Fig. 3A), indicating that h-prune is necessary for cell migration. Expression of the C-terminal region of Myc-h-prune in HeLa S3 cells inhibited the formation of a complex of GSK-3β with h-prune at the endogenous levels, and the cells expressing the Myc-h-prune mutant (C1 and C33) exhibited slow migration (Fig. 3B). These results suggest that the binding of GSK-3 and h-prune is involved in cell migration.

Localization of h-prune to focal adhesions. To clarify the mode of regulation of cell migration by GSK-3 and h-prune, the subcellular localization of these proteins was examined. GSK-3β was observed to be localized along with stress fibers in HeLa S3 cells when the cells were treated with 0.5% Triton X-100 to remove soluble proteins (Fig. 4A, a to c). h-prune was located at focal adhesions at the cell bottom, where paxillin was present, and these two proteins were colocalized (Fig. 4A, d to f). Similar subcellular localizations of these two proteins were also observed in C57MG mouse mammary gland cells (Fig. 4B, a to c and m to o). GSK-3β was located to stress fibers, and GSK-3β on the ends of stress fibers was colocalized with paxillin at focal adhesions (Fig. 4B, a to f). Furthermore, the Tyr216-phosphorylated form of GSK-3β was present at the terminal regions of stress fibers (Fig. 4B, g to i), consistent with previous observations (3). h-prune was observed on the ends of stress fibers at focal adhesions and colocalized with paxillin (Fig. 4B, j to o). h-prune and GSK-3 were partially colocalized to the ends of stress fibers at focal adhesions (Fig. 4B, p to r). h-prune and vinculin, another focal adhesion protein, were also clearly colocalized to focal adhesions at the cell bottom (data not shown). Consistent with these results, immunoprecipitation assays demonstrated that h-prune is associated with paxillin and vinculin in addition to GSK-3β at the endogenous levels in HeLa S3 (data not shown) and C57MG (Fig. 4C) cells. Myc-h-prune(1-332) but not Myc-h-prune(333-453) or Myc-h-prune(199-453) interacted with paxillin (Fig. 4D), indicating that GSK-3 and paxillin form a complex with different regions of h-prune. Furthermore, recombinant GST-paxillin precipitated h-prune, vinculin, and GSK-3β from the HeLa S3 cells expressing Myc-h-prune (Fig. 4E). Taken together, these results suggest that h-prune links active GSK-3 to focal adhesions.

Involvement of GSK-3 and h-prune in formation of focal adhesions. The scratch wound migration assay was performed

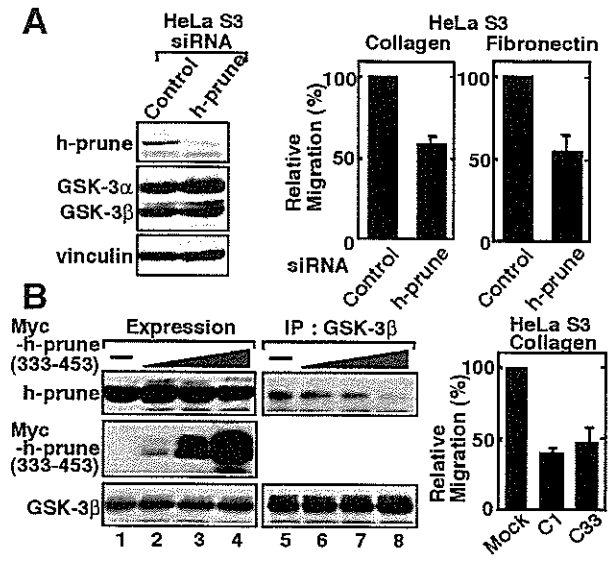

FIG. 3. Involvement of h-prune in cell migration. (A) Left panel, the lysates of HeLa S3 cells transfected with control siRNA or siRNA for h-prune were probed with the indicated antibodies. Right panel, HeLa S3 cells transfected with control siRNA or siRNA for h-prune were subjected to the Transwell migration assay. (B) Left panel, the lysates of HeLa S3 cells expressing Myc-h-prune(333-453) were probed with anti-h-prune or anti-GSK-3β antibody (lanes 1 to 4). The same lysates were immunoprecipitated with anti-GSK-3β antibody (lanes 5 to 8). Right panel, two different clones (C1 and C33) of HeLa S3 cells stably expressing Myc-h-prune(199-453) were subjected to the Transwell migration assay. Cells transfected with vectors alone were used as a control (Mock). The results shown are means ± standard errors of the means from three independent experiments. IP, immunoprecipitation.

to examine the roles of GSK-3 and h-prune in the formation of focal adhesions. C57MG cells were allowed to migrate in scratch wound cultures, resulting in wound closure after 12 h, which was inhibited by SB216763 (Fig. 5A). Paxillin and vinculin were observed clearly in control migrating cells, and h-prune was colocalized with them (Fig. 5B, a to c and j to l). Large focal adhesions, including paxillin, vinculin, and h-prune, were formed at a leading edge of the cells treated with SB216763 (Fig. 5B, d to f, m to o). These proteins seemed to be accumulated at focal adhesions in the treated cells compared with control cells. Dipyridamole did not affect the subcellular localization of paxillin and h-prune (Fig. 5B, g to i), indicating that the PDE activity is not required for the localization of h-prune to focal adhesions. h-prune accumulated in the cells treated with SB216763 was localized to the tips of actin fibers (data not shown). To perform similar experiments with RNAi, we analyzed HeLa S3 cells. At the cell front along the leading edge of migrating HeLa S3 cells, weak staining of paxillin and vinculin was detected and little h-prune was observed (Fig. 5C, a to c and g to i). GSK-3β knocked-down cells exhibited the accumulation of paxillin, vinculin, and h-prune at focal adhesions (Fig. 5C, d to f and j to l).

Inhibition of GSK-3 activity did not affect the expression level of h-prune (Fig. 2E). Since it has been suggested that the formation of large focal adhesions is due to the reduced turnover of adhesions (36), the effects of GSK-3 and h-prune on

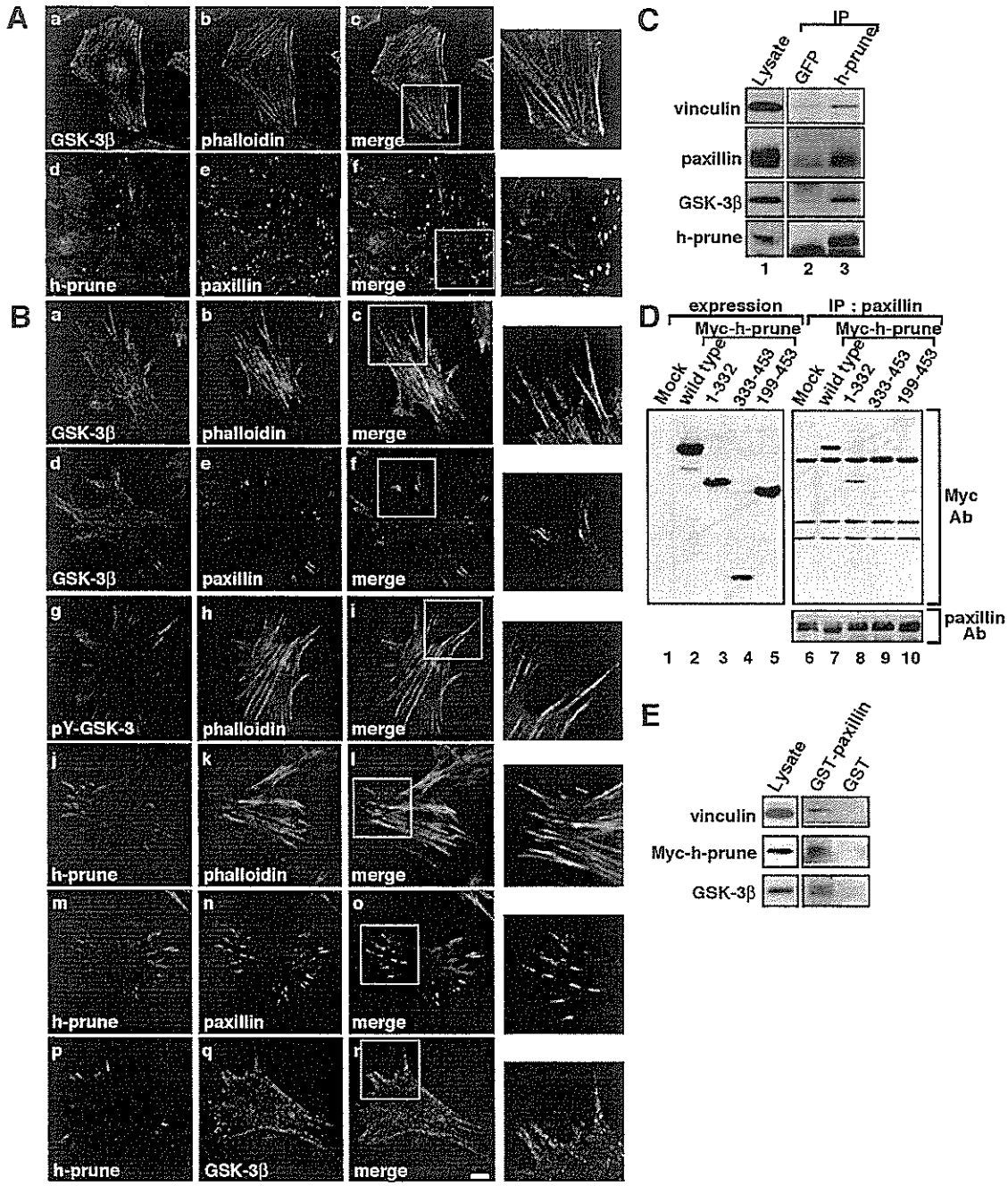

FIG. 4. Localization of h-prune and GSK-3 to focal adhesions. (A) HeLa S3 cells were stained with anti-GSK-3β (a), anti-h-prune (d), or antipaxillin (e) antibody or phalloidin-fluorescein isothiocyanate (FITC) (b). Merged images are shown in panels c and f. The regions in white boxes are shown magnified. (B) C57MG cells were stained with anti-GSK-3β (a and d), anti-pY216-GSK-3β (g), anti-h-prune (j, m, and p), or antipaxillin (e and n) antibody or phalloidin-FITC (b, h, and k). To show the localization of GSK-3 and h-prune simultaneously, anti-GSK-3 antibody was labeled with a Zenon labeling kit (Molecular Probes) (q). Merged images are shown in panels c, f, i, l, o, and r. The regions in white boxes are shown magnified. Scale bar, 10 μm. (C) The lysates of C57MG cells (lane 1) were immunoprecipitated with anti-h-prune antibody, and the immunoprecipitates were probed with the indicated antibodies (lane 3). The immunoprecipitates obtained with anti-GFP antibody were used as a control (lane 2). (D) The lysates of COS cells expressing deletion mutants of h-prune were probed with anti-Myc antibody (lanes 1 to 5). The same lysates were immunoprecipitated with antipaxillin antibody, and the immunoprecipitates were probed with the indicated antibodies (lanes 6 to 10). The results shown are representative of three independent experiments. (E) HeLa S3 cells expressing Myc-h-prune were lysed, and the lysates were incubated with 0.1 μM GST-paxillin or GST immobilized on glutathione-Sepharose. After GST-paxillin or GST was precipitated by centrifugation, the precipitates were probed with the indicated antibodies. IP, immunoprecipitation; Ab, antibody; Mock, control.

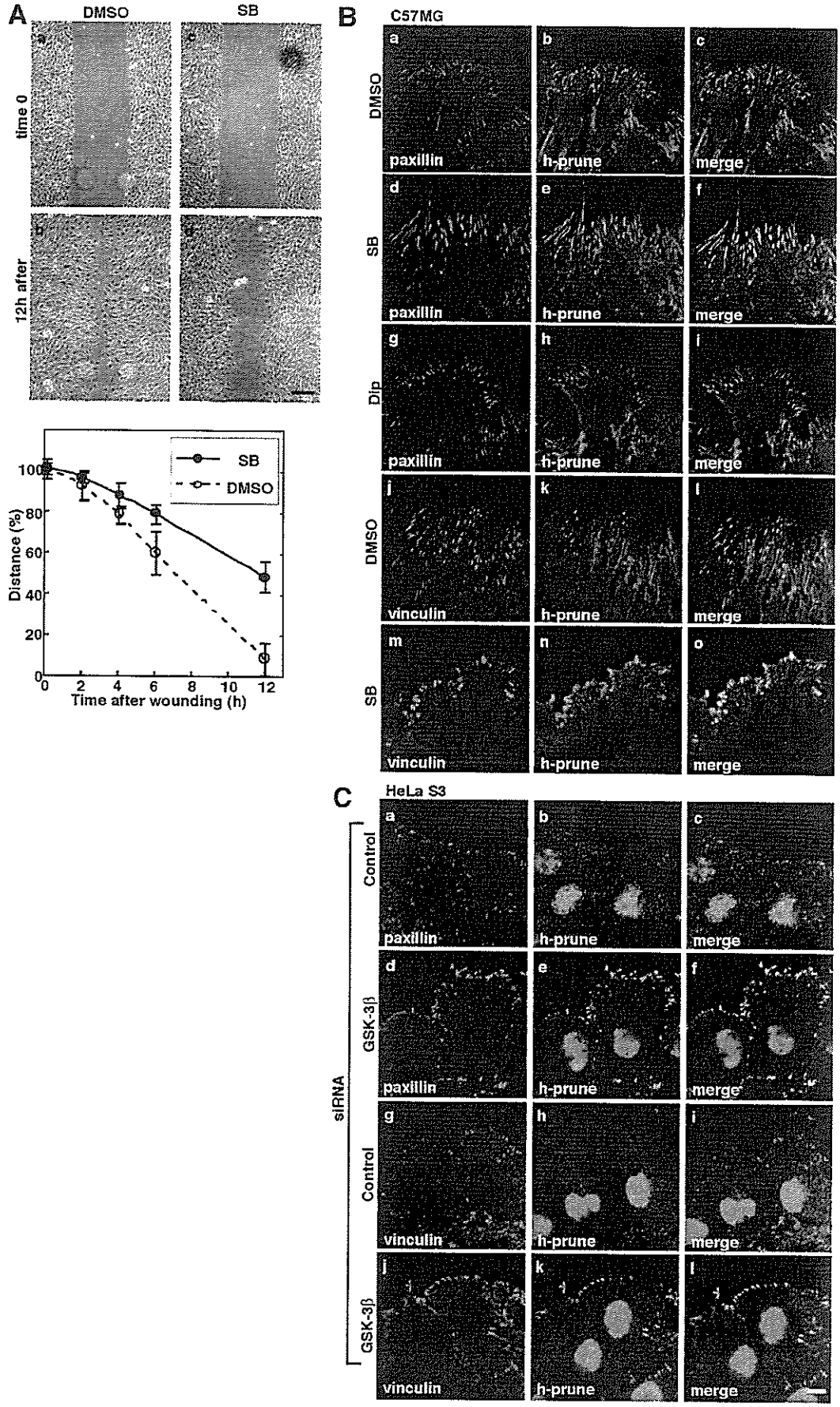
A
DMSO
SB
time 0
12h after
a
c
b
d
SB
DMSO
Distance (%)
Time after wounding (h)
B
C57MG
DMSO
SB
Dip
DMSO
SB
paxillin
h-prune
merge
vinculin
C
HeLa S3
siRNA
Control
GSK-3β
Control
GSK-3β

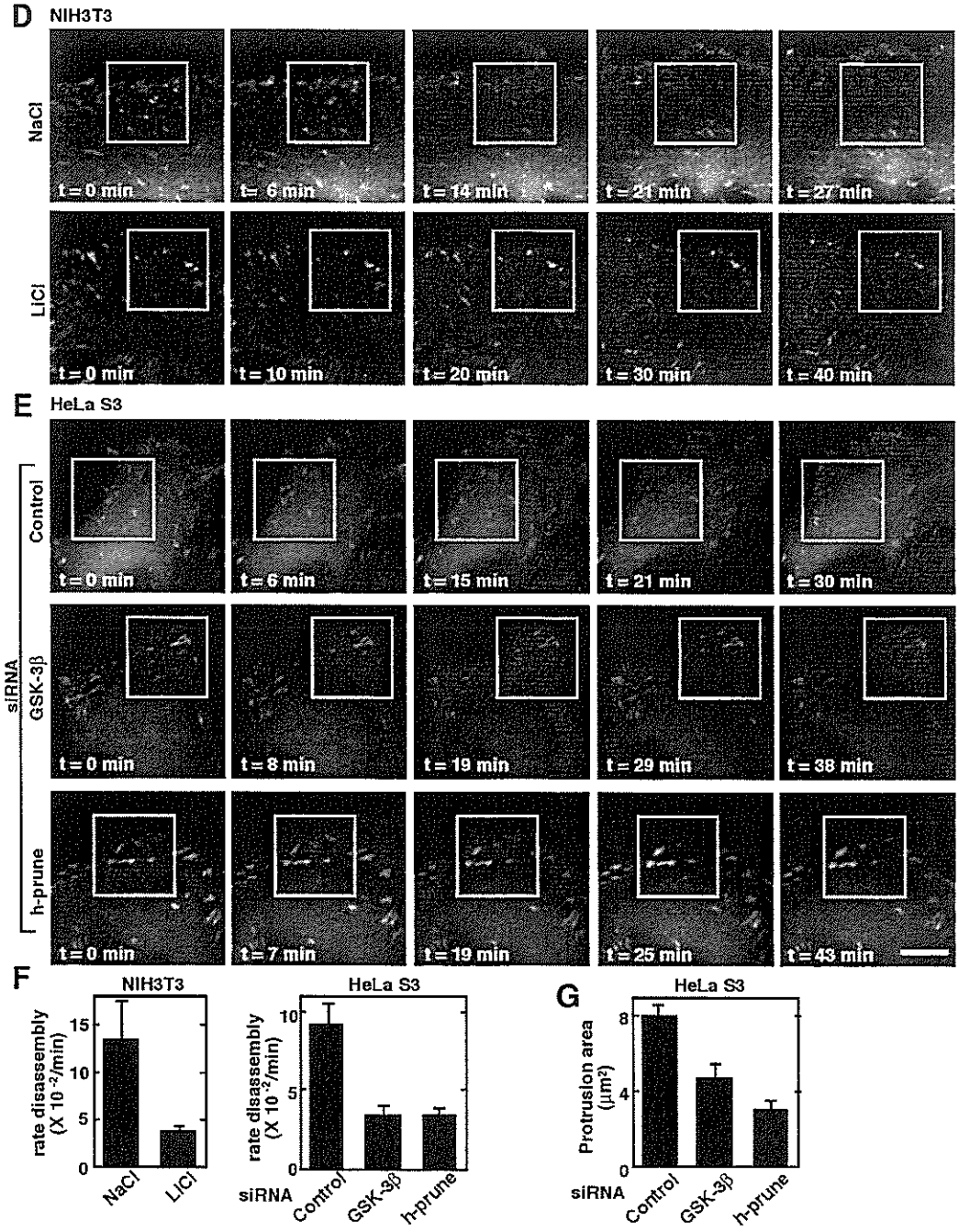

FIG. 5. Involvement of GSK-3 and h-prune in dynamics of focal adhesions. (A) Upper panel, monolayers of C57MG cells on collagen-coated coverslips were treated with 10 μM SB216763 for 4 h. After wounding, wounded monolayers were allowed to heal for 12 h. Scale bar, 0.2 mm. Lower panel, the length of the wounds was measured and expressed as a percentage of the initial distance at time zero. Open circles, dimethyl sulfoxide (DMSO) treatment; filled circles, SB216763 (SB) treatment. The results shown are means ± standard errors of the means from three independent experiments. (B) C57MG cells treated with 10 μM SB216763 (d to f, m to o) or 10 μM dipyridamole (Dip) (g to i) were wounded. Six hours after wounding, the cells were stained with antipaxillin (a, d, and g), antivinculin (j and m), or anti-h-prune (b, e, h, k, and n) antibody. Merged images are shown in panels c, f, i, l, and o. (C) HeLa S3 cells transfected with the siRNA for GSK-3β (d to f and j to l) were wounded. Twelve hours after wounding, the cells were stained with antipaxillin (a and d), antivinculin (g and j), or anti-h-prune (b, e, h, and k) antibody. Merged images are shown in panels c, f, i, and l. Scale bar, 10 μm. The results shown are representative of three independent experiments. (D and E) Dynamics of GFP-paxillin in migrating NIH 3T3 cells treated with NaCl or LiCl (D) and those in HeLa S3 cells treated with the indicated siRNAs (E) were visualized by time-lapse fluorescence microscopy. For each sequence, "t = 0 min" is the frame in which the adhesions in the white box were clearly observed. Scale bar, 5 μm. (F) Rate constants for disassembly of GFP-paxillin in Fig. 5D and E were calculated. Quantifications of GFP-paxillin disassembly show means ± standard errors of the means. (G) The lamellipodium protrusion area was quantified in HeLa S3 cells transfected with siRNA for GSK-3β or h-prune.

the dynamics of focal adhesions were examined. We expressed GFP-paxillin in NIH 3T3 and HeLa S3 cells and analyzed the turnover of adhesions by live fluorescence imaging. At the cell front, paxillin-containing adhesions disassembled as new adhesions were formed near the leading edge (47). We measured the rate constant of disassembly of paxillin-containing adhesions in migrating NIH 3T3 cells and found that the average rate of disassembly of GFP-paxillin from adhesion sites was decreased in LiCl-treated cells (Fig. 5D and F) (see Video S1 in the supplemental material). The rate constants of disassembly of paxillin in NaCl-treated and LiCl-treated cells were $(13.5 \pm 4) \times 10^{-2}\ \mathrm{min}^{-1}$ and $(3.9 \pm 0.4) \times 10^{-2}\ \mathrm{min}^{-1}$, respectively. We also found that the average rate of disassembly of GFP-paxillin was reduced in the GSK-3β or h-prune knocked-down cells (Fig. 5E and F) (see Video S2 in the supplemental material). The rate constants of disassembly of paxillin in control RNA-treated cells, GSK-3β knocked-down cells, and h-prune knocked-down cells were $(9.3 \pm 1.4) \times 10^{-2}\ \mathrm{min}^{-1}$, $(3.4 \pm 0.6) \times 10^{-2}\ \mathrm{min}^{-1}$, and $(3.4 \pm 0.5) \times 10^{-2}\ \mathrm{min}^{-1}$, respectively. Lamellipodia at cell fronts were quantified by measuring the area of protrusion. Lamellipodium protrusion formation was reduced in GSK-3β or h-prune knocked-down cells (Fig. 5G). Taken together, these results suggest that both GSK-3 and h-prune are necessary for the efficient disassembly of adhesion complexes.

Involvement of GSK-3 and h-prune in activation of FAK and Rac. It has been reported that fibroblasts lacking FAK have a reduced migration rate, with an increase in the number and size of peripherally localized adhesions (22, 46). Several tyrosine residues become phosphorylated upon FAK activation (34, 50). FAK is activated via autophosphorylation at Tyr397, which is initiated by integrin engagement with its ligand (38). Therefore, to examine the roles of GSK-3 and h-prune in the activation of FAK, integrin was activated by attaching HeLa S3 cells to collagen. Phosphorylation of Tyr397 of FAK by stimulation with collagen was decreased in GSK-3β and h-prune knocked-down cells (Fig. 6A). Overexpression of h-prune(199-453), which inhibits the interaction of GSK-3 with h-prune, also suppressed the phosphorylation of Tyr397 of FAK (Fig. 6B). These results suggest that FAK acts downstream of GSK-3. Consistent with these observations, expression of $\mathrm{FAK}^{\mathrm{K578E/K581E}}$, a constitutively active form of FAK (15), partially rescued the inhibition of migration in GSK-3β knocked-down cells (Fig. 6C). We next examined the roles of GSK-3 and h-prune in the activation of the small G protein Rac, which stimulates cell migration. Collagen-dependent activation of Rac was suppressed by reducing GSK-3β and h-prune in HeLa S3 cells or by inhibiting GSK-3 activity (Fig. 6C). Rac was activated by scratch wound, and this scratch-induced Rac activation was also suppressed in HeLa S3 cells treated with SB216763 (Fig. 6E). Taken together, these results suggest that GSK-3 and h-prune regulate the activation of FAK and Rac cooperatively.

Correlation of h-prune expression with tumor aggressiveness. h-prune has been reported to be highly expressed in breast cancer (8, 55). We verified the expression of h-prune in other tumors, such as colorectal and pancreatic cancers. Although nonneoplastic colorectal epithelium contained some h-prune-positive cells, cancer tissue gave stronger and more extensive staining (Fig. 7A, a and b). Results were considered positive when more than 50% of the cells were stained. In total, 27 (29.3%) of 92 colorectal cancer cases were positive for h-prune. The positivity of h-prune was correlated with the advanced T grade (depth of invasion), N grade (degree of lymph node metastasis), and M grade (distant metastasis) ($P = 0.0132$, $P = 0.0044$, and $P = 0.0215$, respectively; Fisher's exact test) (Table 1). Moreover, h-prune staining was observed more frequently in stage III/IV cases than in stage I/II cases ($P = 0.0044$). Similar findings were also observed in the cases of pancreatic cancer (18/42 cases were positive) except for M grade cases (Fig. 7A, c and d, and Table 2). There was no significant association between h-prune expression and M grade, but pancreatic cancer cases with distant metastasis had a tendency to express h-prune more strongly than those without distant metastasis. These findings suggest that highly expressed h-prune could be generally related to higher tumor aggressiveness.

As seen in other cell lines, h-prune was colocalized with paxillin at focal adhesions in SW480 colorectal cancer-derived cells (Fig. 7B). In scratch wound culture, treatment of SW480 cells with SB216763 or the siRNA for GSK-3β or h-prune caused the accumulation of paxillin at the leading edge (Fig. 7C). Reduction of GSK-3 or h-prune by RNAi inhibited the migration of SW480 cells (Fig. 7D). Consistent with previously reported observations (8), dipyridamole suppressed the migration of SW480 cells (Fig. 7E). Furthermore, SB216763 and dipyridamole inhibited cell migration additively (Fig. 7E), suggesting that the combination of the inhibitors for the h-prune PDE activity and GSK-3 kinase activity prevents invasiveness or metastasis of colorectal cancer.

DISCUSSION

Cell migration is a complex cellular behavior that involves protrusion and adhesion at the cell front and contraction and detachment at the rear (36). In this study, we provide evidence that GSK-3 and h-prune regulate cell migration cooperatively. Treatment of the cells with GSK-3 inhibitors induced the dissociation of GSK-3 from h-prune and suppressed cell migration. Knockdown of GSK-3 or h-prune by RNAi also inhibited cell migration. Furthermore, expression of the C-terminal region of h-prune in HeLa S3 cells inhibited the interaction of GSK-3 with h-prune and cell migration. Although we cannot exclude the possibility that overexpression of the C-terminal region of h-prune has other effects, these results suggest that the binding of GSK-3 to h-prune is necessary for cell migration. Furthermore, inhibition of GSK-3 affected both haptotactic and random migration. It has been suggested that haptotactic migration is more dependent on the ability of cells to form adhesive contacts at the cell front and that random migration is more limited by the ability of cells to release adhesions at the cell rear (20). Therefore, GSK-3 plays a role in the assembly and/or disassembly of focal adhesions.

How do GSK-3 and h-prune regulate cell motility? GSK-3 or h-prune knocked-down cells exhibited large focal adhesions. Furthermore, reduction of GSK-3 or h-prune by RNAi impaired the disassembly of paxillin from focal adhesions. Similar phenotypes of abnormal focal adhesions with reduced cell migration are observed in the fibroblasts from mice lacking FAK (22). FAK activation, demonstrated by an increase in the phosphorylation of Tyr397 in the protein, is best understood in the